Journal of Computational Neuroscience manuscript No.
(will be inserted by the editor)

Bifurcations of Large Networks of Two-Dimensional Integrate and Fire Neurons

Wilten Nicola · Sue Ann Campbell

Received: date / Accepted: date

Abstract Recently, a class of two-dimensional integrate and fire models has been used to faithfully model spiking neurons. This class includes the Izhikevich model, the adaptive exponential integrate and fire model, and the quartic integrate and fire model. The bifurcation types for the individual neurons have been thoroughly analyzed by Touboul (2008). However, when the models are coupled together to form networks, the networks can display bifurcations that an uncoupled oscillator cannot. For example, the networks can transition from firing with a constant rate to burst firing. This paper introduces a technique to reduce a full network of this class of neurons to a mean field model, in the form of a system of switching ordinary differential equations. The reduction uses population density methods and a quasi-steady state approximation to arrive at the mean field system. Reduced models are derived for networks with different topologies and different model neurons with biologically derived parameters. The mean field equations are able to qualitatively and quantitatively describe the bifurcations that the full networks display. Extensions and higher order approximations are discussed.

Keywords Bifurcation Theory · Mean Field · Large Networks · Bursting · Population Density Methods · Integrate and Fire

W. Nicola

University of Waterloo, Department of Applied Mathematics

E-mail: wnicola@uwaterloo.ca

S.A. Campbell

University of Waterloo, Department of Applied Mathematics

E-mail: sacampbell@uwaterloo.ca

1 Introduction

Recently, a class of two-dimensional spiking neuron models has been introduced that can faithfully model action potential generation in real neurons. This general class of models differs from the typical linear/leaky integrate and fire neuron in the sense that the dynamics are nonlinear, and the models display spike frequency adaptation through a recovery variable. Models of this class include the Izhikevich neuron (Izhikevich, 2003), the adaptive exponential (AdEx) neuron (Brette and Gerstner, 2005; Naud et al., 2008), and the quartic integrate and fire neuron (Touboul, 2008). Furthermore, the usual linear integrate and fire neuron can be included in this class when one adds a recovery variable, which is a modification some authors have used (Nesse et al., 2008; La Camera et al., 2004, 2008; van Vreeswijk and Hansel, 2001). The bifurcation analysis for this two-dimensional class of adapting spiking neuron has also been extensively studied (Touboul, 2008).

However, when these neuron models are coupled together in large networks, they display emergent network level bifurcations not present in the isolated neuron model. For example, the linear integrate and fire with spike frequency adaptation and the Izhikevich neuron models have been shown to display bursts in large networks (van Vreeswijk and Hansel, 2001; Dur-e-Ahmad et al., 2012; Nesse et al., 2008; Wu et al., 2012). Unfortunately, these large network bifurcations remain outside the realm of classical bifurcation theory without a suitable means of reducing the large network to an analyzable system.

One means of achieving this reduction is through population density equations. In population density methods, one begins by defining a time varying population density function, whose evolution is determined by a conservation law (Omurtag et al., 2000; Nykamp. and Tranchina, 2000; Apfaltrer et al., 2006; Abbott and van Vreeswijk, 1993; Treves, 1993). While this is technically an approximation of a large network of time varying ordinary differential equations (ODE's) by a time varying partial differential equation (PDE), the PDE is an exact representation in the limit as the network becomes arbitrarily large. At this stage, one either numerically solves the partial differential equation, or makes further analytical or approximate reductions. For example, one can derive ODE's for the various moments of the density function (Ly and Tranchina, 2007), or try to resolve the spectrum of eigenvalues for the PDE, among other analytical treatments (Abbott and van Vreeswijk, 1993; van Vreeswijk, 1996; Strogatz and Mirollo, 1991; Sirovich et al., 2000; Knight, 2000; Sirovich et al., 2006). It is often the case that this PDE is too complicated to be amenable to direct bifurcation analysis. This is particularly true when we are dealing with neural models of dimension larger than one.

However, a population density approach provides a useful stepping stone to arriving at a mean field approximation to a large network of adapting neurons. In particular, we shall show in this paper that under a separation of time scales and averaging of the adaptation variable, one can rigorously derive a quasi-steady-state approximation of the resulting population density equation of a large network. This results in a system of autonomous switching ODE's that can be analyzed using classical bifurcation theory, in conjunction with the recently developed bifurcation theory of non-smooth systems (di Bernardo et al., 2008). A quasi-steady state approximation to a large network of neurons has been suggested by Ly and Tranchina (2007) and Sirovich et al. (2000), although to our knowledge it has never been used for the purpose of bifurcation analysis for the kinds of two-dimensional neurons we are considering. A similar idea does appear in the work of Nesse et al. (2008). However, the behavior and analysis of the linear integrate and fire network in their work is based on synaptic noise. Mean-field models for uncoupled networks with stochastic noise have also been derived (La Camera et al., 2004, 2008). The neuronal model used in these studies were also adapting and the authors derive a mean-field equation for their adaptation variable, however, the primary goal of the these studies was to derive a firing response for a stochastic adapting neuron. Slightly further from our work is that of Vladimirski et al. (2008), who derive a mean-field equation for a network of homogeneous linear integrate and fire neurons with synaptic depression and noise. Finally, we note the work of Wu et al. (2012) who derive a mean field model for a network with hormone mediated excitability and stochastic synapses, and use it to study network induced bursting. The networks we analyze are entirely deterministic and homogeneous, and the quasi-steady state approximation we arrive is closer to Tikhonov's theorem from dynamical systems (Tikhonov, 1952).

The plan of our article is as follows. Section 1.1 introduces the specific neuron models and networks that we wish to analyze in this paper. Section 2.1 introduces population density methods and section 2.2 introduces moment closure methods as a means of simplifying the population denisty equation. In sections 2.3, we employ a sequence of approximations and assumptions, including the quasi-steady state approximation, to arrive at a system of switching ODE's from the moment-closure reduced population density equation. These ODEs are the mean field equations for the original network. In section 3 we apply this approach to three numerical examples. The first example, studied in section 3.1, is a homogeneous all-to-all coupled Izhikevich network. Section 3.2 considers a network of Izhikevich neurons split into two populations, one strongly adapting, and the other weakly adapting. Both populations are all to all coupled

both internally and externally. Finally, section 3.3 studies a network of AdEx neurons consisting of two populations, one excitatory and one inhibitory with the same network topology as the network studied in section 3.2. Whenever possible, the parameters used in the numerical examples are a result of fitting to actual neuronal data by various authors. In all examples the isolated neurons have two states: quiescent or tonically firing; they are not intrinsically bursting. In section 4, we conclude by discussing the sufficient requirements for our approach to be valid and outline what can be done to extend this approach when these requirements cannot be met. Possible extensions to more realistic types of networks are also discussed in addition to a comparison with other mean-field approaches.

1.1 Modeling Networks of Neurons as Large Networks of Pulse-Coupled Integrate and Fire Neurons

We will consider integrate and fire models consisting of a two-dimensional system of ODEs of the form:

$$v' = F(v) - w + I \tag{1}$$

$$w' = a(bv - w), \tag{2}$$

supplemented by the following discontinuities

$$v(t^-_{spike}) = v_{peak} \quad \Rightarrow \quad \begin{array}{l} v(t^+_{spike}) = v_{reset}, \\ w(t^+_{spike}) = w(t^-_{spike}) + w_{jump}. \end{array} \tag{3}$$

Here v represents the nondimensionalized membrane potential and w is a nondimensionalized current that serves as an adaptation variable. Time has also been non-dimensionalized.

The networks we consider will be coupled together through synaptic currents:

$$I_{\text{syn},ij} = \bar{g}_{ij} s_{ij}(t)(e_r - v_i)$$

where $\bar{g}_{ij}$ is the maximal synaptic conductance and $s_{ij}(t)$ represents the proportion of ion channels open in the membrane of neuron i as a result of the firing in neuron j. The total synaptic current in neuron i due to the presynaptic neurons $j = 1, 2 \ldots N$ is then

$$I_{\text{syn},i} = \sum_{j=1}^{N} \bar{g}_{ij} s_{ij}(t)(e_r - v_i).$$

We assume all-to-all connectivity between different populations and within each population, hence we take $\bar{g}_{ij} = \frac{\bar{g}_i}{N}$ where $\bar{g}_i$ is the maximal synaptic conductance of neuron i. Then the synaptic conductance of

neuron i due to the presynaptic neurons $j = 1, 2 \ldots N$ is given by

$$g_i(t) = \bar{g}_i s_i(t) = \frac{\bar{g}_i}{N} \sum_{j=1}^{N} s_{ij}(t), \tag{4}$$

where $s_i(t)$ is the proportion of ion channels open in the membrane of neuron i due to all presynaptic neurons. Since $s_i(t)$ is a proportion, it should be bounded by 1. This bound is implemented in all numerical simulations. Under the assumption of all-to-all connectivity, $s_i(t) = s(t)$, as every post synaptic neuron receives the same summed input from all the presynaptic neurons. We will assume that $\bar{g}_i = g$, for all i within a population of neurons.

The time variation of $s_{ij}(t)$ will be modeled as transient pulses that occur after a spike. That is, if neuron j fires its kth action potential at time $t = t_{j,k}$, then the variable $s_{ij}(t)$ at time t is given by

$$s_{ij}(t) = \sum_{t_{j,k}<t} E(t - t_{j,k}). \tag{5}$$

There are different functions proposed for $E(t)$ in the literature. Examples include the single exponential synapse:

$$E(t) = s_{jump} \exp\left(\frac{-t}{\tau_s}\right), \tag{6}$$

the double exponential synapse:

$$E(t) = \frac{1}{\tau_D - \tau_R}\left(\exp\left(\frac{-t}{\tau_D}\right) - \exp\left(\frac{-t}{\tau_R}\right)\right), \tag{7}$$

and the alpha synapse

$$E(t) = \alpha^2 t \exp(-\alpha t). \tag{8}$$

With any of these functions, the synaptic coupling function $s(t)$, in the case of all-to-all connectivity (and other cases), can be formally described by a linear system of ordinary differential equations with a sum of delta pulses on the right hand side corresponding to the times a neuron in the network fires a spike. For example, the simple exponential synapse is governed by the ordinary differential equation

$$\frac{ds(t)}{dt} = -\frac{s}{\tau_s} + \frac{s_{jump}}{N} \sum_{j=1}^{N} \sum_{t_{j,k}<t} \delta(t - t_{j,k}). \tag{9}$$

The alpha function synapse and the double exponential synapse have a system of two coupled first order ODEs that describe their dynamics and can be derived in the same manner as the single exponential synapse. For reference purposes, these systems are:

$$\frac{ds}{dt} = -\frac{s(t)}{\tau_R} + h \tag{10}$$

$$\frac{dh}{dt} = -\frac{h}{\tau_D} + \frac{1}{N\tau_R\tau_D} \sum_{j=1}^{N} \sum_{t_{j,k}<t} \delta(t - t_{j,k}) \tag{11}$$

for the double exponential synapse and

$$\frac{ds}{dt} = -\alpha s(t) + h \tag{12}$$

$$\frac{dh}{dt} = -\alpha h + \frac{\alpha^2}{N}\sum_{j=1}^{N}\sum_{t_{j,k}<t}\delta(t - t_{j,k}) \tag{13}$$

for the alpha synapse. One should note that all these ordinary differential equations are linear, and they all contain the term

$$j(t) = \frac{1}{N}\sum_{j=1}^{N}\sum_{t_{j,k}<t}\delta(t - t_{j,k}). \tag{14}$$

This term is very important in the large network dynamics and represents a kind of network averaged firing rate as we will show in section 2.1.

In summary, the model of a network of all-to-all coupled neurons that we will consider is given by system of discontinuous ODE's

$$v_i' = F(v_i) - w_i + I + gs(e_r - v_i) \tag{15}$$

$$w_i' = a(bv_i - w_i) \tag{16}$$

$$v_i(t_{spike}^-) = v_{peak} \quad \Rightarrow \quad \begin{array}{l} v_i(t_{spike}^+) = v_{reset} \\ w_i(t_{spike}^+) = w_i(t_{spike}^-) + w_{jump}, \end{array} \tag{17}$$

for $i = 1, 2, \ldots N$, and where the dynamics of $s(t)$ depend on the specific synapse implemented. A similar set of equations can also be written for multiple coupled populations of neurons within a network. For the purpose of subsequent sections, we will define $\mathbf{x}_i = (v_i, w_i)$, and denote equations (15)–(16) in vector form as

$$\mathbf{x}_i' = \mathbf{G}(\mathbf{x}_i) = \begin{pmatrix} G_1(v_i, w_i, s) \\ G_2(v_i, w_i) \end{pmatrix} = \begin{pmatrix} F(v_i) - w_i + I + gs(e_r - v_i) \\ a(bv_i - w_i) \end{pmatrix}. \tag{18}$$

2 Model Reduction

The model derived in the previous section can be complicated to analyze if N is large. Thus, in this section we will introduce a simpler model that can be used to approximate the behaviour of the full network. This model is actually a partial differential equation that describes the time evolution of the equations (15)-(17) in the limit $N \to \infty$. After a brief departure to discuss firing rates we derive an appropriate mean field synaptic equation in the large N limit. This results in a "typical" population density model, consisting of a PDE coupled to an ODE, with the slight twist that the PDE depends on two variables. Next we show

how a moment closure approach can be used to replace the PDE with one dependent only on the voltage variable and a second ODE for the mean adaptation current. Finally, we introduce a quasi-steady state approximation to eliminate the PDE and derive a pair of non-smooth/switching ODEs for the mean field synaptic and adaptation variables.

2.1 Population Density Methods

One way to analyze large systems with quantities that are conserved is the continuity equation or population density equation. This equation applies to neural networks since the total number of neurons in a network is a conserved quantity. In order to apply it, we need to define a density function. Using the notation introduced in the previous section, we take the phase space $\mathbf{X}$ consisting of vectors $\mathbf{x} = (v, w)$. Note that we are not considering the synaptic components as part of phase space. Their incorporation will follow in the subsequent section. Now consider a region Ω in phase space with piecewise smooth boundary. Let $P(\Omega, t)$ be the proportion of neurons in Ω at time t. In the "large network limit", we can define the population density function, $\rho(\mathbf{x}, t)$ as follows

$$P(\Omega, t) = \lim_{N\to\infty} \sum_{i=1}^{N} \chi_\Omega(\mathbf{x}_i) = \int_{\mathbf{X}} \chi_\Omega(\mathbf{x})\rho(\mathbf{x}, t)\, d\mathbf{x} = \int_\Omega \rho(\mathbf{x}, t)\, d\mathbf{x}. \tag{19}$$

where χ_Ω is the conventional indicator function. The time evolution of the probability density function ρ is simply a conservation equation, often called the continuity equation, given by

$$\frac{\partial \rho}{\partial t} = -\nabla \cdot \mathbf{J}(\mathbf{x}, t). \tag{20}$$

where $\mathbf{J}(\mathbf{x}, t) = \mathbf{G}(\mathbf{x})\rho(\mathbf{x}, t)$ is the flux. In the case we are considering, the flux is a vector of two components, $\mathbf{J}(\mathbf{x}, t) = (J_V(v, w, s, t), J_W(v, w, t))$. Note, from the definition of $\mathbf{G}(\mathbf{x})$ (see (18)), that J_V is s dependent. The flux is particularly interesting as it is intuitively the mass (proportional) flow rate along a specific direction in phase space. Additionally, any resets in the neural model are incorporated into boundary conditions defined in terms of the flux. In our model, the reset (17) becomes the boundary condition

$$J_V(v_{peak}, w, s, t) = J_V(v_{reset}, w + w_{jump}, s, t). \tag{21}$$

In the context of neuroscience, there are derivations of equation (20) contained in various sources (Omurtag et al., 2000; Nykamp. and Tranchina, 2000). The continuity equation has been used to analyze the stability of the asynchronous state of a network of one dimensional non-adapting coupled neurons

(predominantly integrate and fire) by various authors (van Vreeswijk, 1996; Strogatz and Mirollo, 1991; Abbott and van Vreeswijk, 1993; Sirovich et al., 2006; van Vreeswijk et al., 1994). Another use is to eliminate the need for direct simulation of large networks, instead numerically solving the continuity equation (Omurtag et al., 2000; Nykamp. and Tranchina, 2000; Ly and Tranchina, 2007; Apfaltrer et al., 2006). The specific application of the continuity equation to neurons that are governed by more complicated dynamics than a single differential equation is limited (Casti et al., 2002). It should be noted that the system analyzed by Casti et al. (2002) is a network of linear integrate-and-fire or burst neurons, neurons that intrinsically burst due to their underlying dynamics, not due to the effect of network connectivity. More analytical treatments of the partial differential equation (20), including solving for the steady state, resolving its spectrum of eigenvalues, and studying its properties as a linear operator can be found in Abbott and van Vreeswijk (1993); van Vreeswijk (1996); Strogatz and Mirollo (1991); Sirovich et al. (2000); Knight (2000) and Sirovich et al. (2006).

To complete our population density model we need to consider the large network limit of the model for the synaptic coupling. It can be shown (see Appendix) that the following holds

$$\lim_{N\to\infty} j(t) = \lim_{N\to\infty} \frac{1}{N} \sum_{j=1}^{N} \sum_{t_{j,k}<t} \delta(t - t_{j,k}) = \langle R_i(t) \rangle = \int_W J_V(v_{peak}, w, s, t)\, dw. \tag{22}$$

Here $\langle R_i(t) \rangle$ denotes the network averaged instantaneous firing rate, where $\langle\rangle$ corresponds to averaging across the network. Using equation (22), our model is now a PDE coupled to an ODE or system of ODE's. In the case of the simple exponential synapse, we have

$$\frac{\partial \rho(v,w,t)}{\partial t} = -\frac{\partial}{\partial v}\left((F(v) - w + I + gs(e_r - v))\rho(v,w,t)\right) - \frac{\partial}{\partial w}\left(a(bv - w)\rho(v,w,t)\right) \tag{23}$$

$$s' = -\frac{s}{\tau_s} + s_{jump} \int_W J_V(v_{peak}, w, s, t)\, dw. \tag{24}$$

The ordinary differential equations for the double exponential and alpha synapses can be derived in a similar matter, yielding equations where $j(t)$ is replaced with $\langle R_i(t) \rangle$, as given by (22). A similar system of coupled ODEs/PDEs can be derived in the case of multiple distinct populations of neurons. One merely defines a population density equation and flux vector for each population.

The coupled ODE-PDE system (23)–(24) is generally not analytically solvable. Numerical solution of the system is possible, however, this approach will not be pursued here. There is a simpler alternative to numerical solution that can be implemented to determine the bifurcation types this system displays, and yield the approximate bifurcation manifolds. Furthermore, one can easily extend this approach to networks

containing mutiple populations of neurons with different parameters (as we will show in section 3). However, we will first simplify the PDE (23).

2.2 Simplification of the Continuity Equation

In this section we will show how the moment closure assumption (Ly and Tranchina, 2007) can be used to replace the PDE (23) by one where ρ is a function of t and v only and an ODE governing the mean of w. To begin, we write the density in its conditional form

$$\rho(v, w, t) = \rho_W(w|v, t)\rho_V(v, t), \tag{25}$$

and substitute into (23) to obtain

$$\begin{aligned}\frac{\partial}{\partial t}\left(\rho_V(v,t)\rho_W(w|v,t)\right) = &-\frac{\partial}{\partial v}\left((F(v)+I-w+g(e_r-v)s)\rho_V(v,t)\rho_W(w|v,t)\right)\\ &-\frac{\partial}{\partial w}\left(a(bv-w)\rho_V(v,t)\rho_W(w|v,t)\right).\end{aligned} \tag{26}$$

If this equation is integrated with respect to w, terms involving the first order conditional moments $\langle w|v\rangle$ will occur. The first order moment closure method entails making the assumption that $\langle w|v\rangle = \langle w\rangle$. The validity of this assumption at high firing rates is supported by numerical simulations of the full network. These simulations show that when the firing rate is high, w_i tracks the network averaged firing rate much more closely than it follows v_i at any point in time.

Integrating (26) with respect to w over the entire phase space W, using the normalization condition on the density of w, the fact that $\rho_W(w|v)$ is zero on the boundary and the moment closure assumption yields

$$\frac{\partial}{\partial t}\left(\rho_V(v,t)\right) = -\frac{\partial}{\partial v}\left((F(v)-\langle w\rangle+I+g(e_r-v)s)\rho_V(v,t)\right). \tag{27}$$

Integrating the boundary condition (21) with respect to w on W and using the moment closure assumption, we get the corresponding boundary condition for the PDE (27):

$$J(v_{peak}, \langle w\rangle, s, t) = J(v_{reset}, \langle w\rangle + w_{jump}, s, t), \tag{28}$$

where we have dropped the subscript V on J as it is unnecessary.

We now derive an ordinary differential equation for the mean adaptation variable

$$\langle w\rangle = \int_V \int_W w\rho(v, w, t)\, dwdv.$$

Differentiation with respect to time, using the continuity equation (20) and equation (18) yields

$$\langle w\rangle' = -\int_V \int_W w\frac{\partial}{\partial v}\left(\rho(v,w,t)G_1(v,w,s)\right)\,dwdv \;-\int_V \int_W w\frac{\partial}{\partial w}\left(\rho(v,w,t)G_2(v,w)\right)\,dwdv.$$

Applying integration by parts and changing the order of integration as needed then gives:

$$\langle w\rangle' = \langle G_2(v,w)\rangle - \int_W w\rho(v,w,t)G_1(v,w,s)|_{\partial V}\,dw - \int_V wG_2(v,w)\rho(v,w,t)|_{\partial W}\,dv. \tag{29}$$

Note that since $G_2(v,w)$ is linear, $\langle G_2(v,w)\rangle = G_2(\langle w\rangle,\langle v\rangle)$. Then, using $\rho(v,w,t)=0$ on ∂W, the boundary condition (28) and returning to the flux notation, the equation can be rewritten

$$\langle w\rangle' = G_2(\langle w\rangle,\langle v\rangle) - \int_W w\left(J_V(v_{peak},w,s,t) - J_V(v_{peak},w-w_{jump},s,t)\right)\,dw. \tag{30}$$

To proceed further, we assume that $\langle w\rangle \gg w_{jump}$ and apply a Taylor expansion to yield

$$\begin{aligned}\langle w\rangle' &= G_2(\langle w\rangle,\langle v\rangle) - \int_W w\left(w_{jump}\frac{\partial J_V(v_{peak},w,s,t)}{\partial w} + O(w_{jump}^2)\right)\,dw\\ &= G_2(\langle w\rangle,\langle v\rangle) + w_{jump}\int_W J_V(v_{peak},w,s,t)\,dw + O(w_{jump}^2)\end{aligned} \tag{31}$$

Thus the partial differential equation (23) can be replaced by (27) and (31). Note that this can be interpreted as replacing each neuron's adaptation variable with the mean field adaptation, $\langle w\rangle$.

We now have a first order partial differential equation and a pair of coupled ordinary differential equations describing our system:

$$\frac{\partial}{\partial t}\rho(v,t) = -\frac{\partial}{\partial v}\left(\left(F(v) - \langle w\rangle + I + g(e_r-v)s\right)\left(\rho(v,t)\right)\right) \tag{32}$$

$$\langle w\rangle' = a(b\langle v\rangle - \langle w\rangle) + w_{jump}\int_W J_V(v_{peak},w,s,t)\,dw + O(w_{jump}^2) \tag{33}$$

$$s' = -\frac{s}{\tau_s} + s_{jump}\int_W J_V(v_{peak},w,s,t)\,dw, \tag{34}$$

where we have dropped the V subscript on ρ since it is unnecessary. Thus far, everything we have done is exact. One level of approximation comes from dropping all the higher order terms in the expansion in (33), yielding

$$\langle w\rangle' \approx a(b\langle v\rangle - \langle w\rangle) + w_{jump}\int_W J_V(v_{peak},w,s,t)\,dw.$$

Another level of approximation comes from a perturbation argument. When deriving the non-dimensionalized system (1)-(2) from particular dimensional models, we often found that $b \ll 1$, i.e., b can be considered a

small parameter. Thus, our second approximation is a perturbation expansion in b, where we only consider the $O(1)$ problem:

$$\langle w\rangle' \approx -a\langle w\rangle + w_{jump}\int_W J_V(v_{peak}, w, s, t)\, dw.$$

Evaluating the integral of the flux using the moment closure assumption, we obtain the following dynamical system:

$$\frac{\partial}{\partial t}\rho(v,t) = -\frac{\partial}{\partial v}\left((F(v) - \langle w\rangle + I + g(e_r - v)s)\,(\rho(v,t))\right) \tag{35}$$

$$\langle w\rangle' = -a\langle w\rangle + w_{jump}J(v_{peak}, \langle w\rangle, s, t) \tag{36}$$

$$s' = -\frac{s}{\tau_s} + s_{jump}J(v_{peak}, \langle w\rangle, s, t). \tag{37}$$

Note that we can replace the boundary condition (28) with

$$J(v_{peak}, \langle w\rangle, s) = J(v_{reset}, \langle w\rangle, s),$$

as this is consistent with the assumption $\langle w\rangle \gg w_{jump}$.

At this point we need another level of approximation to yield a system that is simple enough to analyze using bifurcation theory. This will take the form of a quasi-steady state approximation, based on a separation of time scales.

2.3 The Quasi-Steady State Approximation

In the type of neural models we are considering, the shortest time scale is typically the membrane time constant and the longest time scale is that of the adaptation variable. However, for inhibitory synapses or certain excitatory synapses, the longest timescale may be that of the s variable (Ermentrout and Terman, 2010). As our starting system (1)-(2) is dimensionless, the membrane potential time constant is 1. Assuming the adaptation time scale is much longer, $a^{-1} = \tau_w \gg 1$, we can regard τ_w^{-1} as a small parameter. Then, introducing the "slow time" $\tilde{t} = \tau_w^{-1}t$, the system becomes

$$\begin{aligned}
\tau_w^{-1}\frac{\partial}{\partial \tilde{t}}\rho(v,\tilde{t}) &= -\frac{\partial}{\partial v}\left((F(v) - \langle w\rangle + I + g(e_r - v)s)\,(\rho(v,\tilde{t}))\right)\\
\frac{d}{d\tilde{t}}\langle w\rangle &= \langle w\rangle + \tau_w w_{jump}J(v_{peak}, \langle w\rangle, s, \tilde{t})\\
\frac{\tau_s}{\tau_w}\frac{ds}{d\tilde{t}} &= -s + \tau_s s_{jump}J(v_{peak}, \langle w\rangle, s, \tilde{t}).
\end{aligned}$$

If $\tau_s = O(\tau_w)$, we can apply a quasi-steady state approximation to the PDE. This entails assuming that the density $\rho(v,t)$ reaches its steady state density $\rho(v)$, rapidly relative to s and $\langle w \rangle$:

$$\begin{aligned} \frac{\partial \rho(v,\tilde{t})}{\partial \tilde{t}} &= 0 \\ &\Rightarrow \left(F(v) - \langle w \rangle + I + g(e_r - v)s\right)(\rho(v)) = J(\langle w \rangle, s), \end{aligned} \tag{38}$$

i.e., the flux is independent of v. If that the network is tonically firing, i.e., the v vector field is strictly non-negative, then we can use the normalization condition on the density to solve for the flux:

$$J(\langle w \rangle, s) = \left[\int_V \frac{dv}{F(v) - \langle w \rangle + I + g(e_r - v)s} \right]^{-1}. \tag{39}$$

Using equation (39) and the ordinary differential equations for $\langle w \rangle$ and s, we now have a closed system of non-linear autonomous ODE's. Hence it would appear that we can use classical bifurcation theory to analyze the resulting bifurcations. However, one has to be careful when the denominator inside the integrand of (39) is not strictly positive on the phase space. If this occurs, then the flux changes sign in the phase space and one can no longer assume the flux is independent of v ($\frac{\partial J}{\partial v} = 0$). For a more intuitive explanation, one can consider the pseudo-neuron with "average" dynamics

$$v' = F(v) - \langle w \rangle + I + g(e_r - v)s, \tag{40}$$

A sign change in the flux corresponds to a saddle-node bifurcation for (40). Regarding s, $\langle w \rangle$ as fixed parameters, we know from the analysis of Touboul (2008) that this bifurcation occurs when

$$I = I^*(\langle w \rangle, s) = \langle w \rangle - \min_v (F(v) + g(e_r - v)s). \tag{41}$$

For $I < I^*(\langle w \rangle s)$, (40) has two fixed points, for $I > I^*(\langle w \rangle, s)$, (40) has no fixed points, and for $I = I^*(\langle w \rangle s)$ has one fixed point. The line $I^*(\langle w \rangle, s)$ thus forms a switching manifold in the phase space of s and $\langle w \rangle$. For $I > I^*(\langle w \rangle, s)$, there are no fixed points and the system is tonically firing. Thus

$$\langle R_i(t) \rangle = J(\langle w \rangle, s) = \left[\int_V \frac{dv}{F(v) - \langle w \rangle + I + g(e_r - v)s} \right]^{-1}, \quad \text{if} \quad I > I^*(\langle w \rangle, s). \tag{42}$$

When the system undergoes the saddle-node bifurcation, solutions approach a stable fixed point, thus it seems reasonable to take the firing rate to be zero:

$$\langle R_i(t) \rangle = 0, \quad \text{if} \quad I \leq I^*(\langle w \rangle, s). \tag{43}$$

This is the assumption we will make in the rest of the paper. In reality, however, things are more subtle. Where the fixed points emerge at the bifurcation and their respective stability have important implications

for the value of $\langle R_i(t)\rangle$. As shown in Figure 1, if an unstable equilibrium point, v_+ emerges in the region $[v_{reset}, v_{peak}]$, a residual firing rate occurs. This is due to the remaining density in the region $[v_+, v_{peak}]$ and the positive flux in this region as $\dot{v} > 0$ for $[v_+, v_{peak}]$. If we simply set $\langle R_i(t)\rangle = 0$ when $I < I^*(\langle w\rangle, s)$, then we do not account for this residual firing rate. We have numerically found that it is small in magnitude for biophysical derived parameters and thus it can be ignored.

In summary, using the quasi-steady state approximation and other assumptions as discussed above, the system (35)-(37) can be reduced to the following switching system of ODEs:

$$\langle w\rangle' = -\frac{\langle w\rangle}{\tau_w} + w_{jump}\langle R_i(t)\rangle \tag{44}$$

$$s' = -\frac{s}{\tau_s} + s_{jump}\langle R_i(t)\rangle \tag{45}$$

where $\langle R_i(t)\rangle$ is given by (42)-(43). We will refer to this system the mean field model.

3 Numerical Examples

We now apply the approach described in the previous section to a set of numerical examples to demonstrate its versatility. We consider three networks with different kinds of synapses, topology, and individual neurons. The first is an all-to-all coupled Izhikevich network with the simple exponential synapse. This network is notable as with strong enough adaptation, it displays a bifurcation to bursting which we analyze using bifurcation theory. We will need the bifurcation theory of non-smooth systems (di Bernardo et al., 2008) to understand the limit cycle associated with bursting, and its emergence/disappearance. The second network we analyze contains two populations of Izhikevich neurons, one strongly adapting, and one weakly adapting. We vary the proportion of neurons of each type in the network, and show how it affects the bifurcation to bursting. The final network we consider consists of inhibitory and excitatory adaptive exponential neurons. The synapses implemented in this network are of the double-exponential kind. The network topologies and neuron types are shown in Figure 2. The code needed to generate direct network simulations, the mean field equations, and any bifurcation diagrams of the mean-field equations has been uploaded to ModelDB (Hines et al., 2002). The accession number for the code is 146499.

3.1 Example 1: The Single All-to-All coupled Izhikevich Network

The dimensional form of this model is given by

$$C\dot{V}_i = k(V_i - V_T)(V - V_R) - W_i + I_{app} + g_{syn}(e_r - V_i)s \tag{46}$$

$$\dot{W}_i = \frac{\eta(V_i - V_R) - W_i}{\tau_W} \tag{47}$$

$$\dot{s} = -\frac{s}{\tau_{syn}} + s_{jump}j(t) \tag{48}$$

$$V_i(t^-_{spike}) = V_{peak} \quad \Rightarrow \quad \begin{aligned} V_i(t^+_{spike}) &= V_{reset} \\ W_i(t^+_{spike}) &= W_i(t^-_{spike}) + W_{jump}, \end{aligned} \tag{49}$$

for $i = 1, 2, \ldots N$. The parameter values can be found in Table 1. With the exception of the parameter k, these values are taken from Dur-e-Ahmad et al. (2012) where they were chosen to fit hippocampal CA3 pyramidal neuron data from various sources, the primary source being (Hemond et al., 2008). In order to fit the right action potential halfwidth, Dur-e-Ahmad et al. (2012) required the value of k to switch depending on the relationship between $V(t)$ and V_T. As this complicates matters somewhat (via an added level of discontinuity), we have instead chosen a single, intermediate value for k. Dur-e-Ahmad et al. (2012) numerically explored the parameter regions for which their model displays bursting. The techniques of the previous sections will allow us to study the bifurcations associated with the transition to bursting in this network.

The dimensionless form of the model is given by

$$v_i' = v_i(v_i - \alpha) - w_i + I + g(e_r - v_i)s \tag{50}$$

$$w_i' = a(bv_i - w_i) \tag{51}$$

$$s' = -\frac{s}{\tau_s} + s_{jump}j(t) \tag{52}$$

$$v_i(t^-_{spike}) = v_{peak} \quad \Rightarrow \quad \begin{aligned} v_i(t^+_{spike}) &= v_{reset} \\ w_i(t^+_{spike}) &= w_i(t^-_{spike}) + w_{jump}, \end{aligned} \tag{53}$$

for $i = 1, \ldots, N$, where

$$v_i = 1 + \frac{V_i}{|V_R|}, \qquad w_i = \frac{W_i}{k|V_R|^2}.$$

Dimensional Parameters		Dimensionless Parameters	
C	250 pF	$\alpha = 1 + \frac{V_T}{\lvert V_R \rvert}$	0.62
k	2.5 nS/mV	$b = \frac{\eta}{k\lvert V_R \rvert}$	0.006
V_R	-65 mV	$I = \frac{I_{app}}{k\lvert V_R \rvert^2}$	0.14
V_T	$V_r + 40 - \frac{b}{k} = 41.7$mV	$g = \frac{g_{syn}}{k\lvert V_R \rvert}$	1.23
V_{peak}	30 mV	$a = \left(\frac{\tau_W k\lvert V_R \rvert}{C}\right)^{-1}$	0.015
V_{reset}	-55 mV	$\tau_s = \frac{\tau_{syn} k\lvert V_R \rvert}{C}$	1.3
W_{jump}	200 pA	$w_{jump} = \frac{W_{jump}}{k\lvert V_R \rvert^2}$	0.0189
τ_W	100 ms		
η	-1 nS		
I_{app}	1500 pA		
g_{syn}	300 nS		
s_{jump}	0.8		
τ_{syn}	2 ms		
N	1000		

Table 1: Parameters (from Dur-e-Ahmad et al. (2012)) for the all-to-all coupled Izhikevich network in numerical example 1. These parameters apply unless otherwise indicated.

The dimensionless parameters are defined in Table 1. Applying the theory in the previous section, we have the following system of switching ordinary differential equations for $s, \langle w \rangle$:

$$\langle w \rangle' = -\frac{\langle w \rangle}{\tau_w} + w_{jump}\langle R_i(t) \rangle \tag{54}$$

$$s' = -\frac{s}{\tau_s} + s_{jump}\langle R_i(t) \rangle \tag{55}$$

$$\langle R_i(t) \rangle = \begin{cases} \left(\int_V \frac{dv}{v(v-\alpha) - \langle w \rangle + I + g(e_r - v)s} \right)^{-1}, & I \geq I^*(\langle w \rangle, s) \\ 0 & I < I^*(\langle w \rangle, s) \end{cases} \tag{56}$$

$$I^*(\langle w \rangle, s) = \langle w \rangle + \frac{(\alpha + gs)^2}{4} - ge_r s. \tag{57}$$

Note that in this case, we can evaluate $\langle R_i(t) \rangle$ explicitly:

$$\langle R_i(t) \rangle = \begin{cases} \frac{\sqrt{I - I^*(\langle w \rangle, s)}}{\arctan\left(\frac{v_{peak} - \frac{\alpha+gs}{2}}{\sqrt{I - I^*(\langle w \rangle, s)}}\right) - \arctan\left(\frac{v_{reset} - \frac{\alpha+gs}{2}}{\sqrt{I - I^*(\langle w \rangle, s)}}\right)}, & I \geq I^*(\langle w \rangle, s) \\ 0 & I < I^*(\langle w \rangle, s) \end{cases} \tag{58}$$

Simulation of this system of equations was done using MATLAB's ODE45 function (MATLAB, 2012), with the default numerical integration parameter values. The model parameters for all simulations are

found in Table 1, unless otherwise specified in a figure. As can be seen in Figure 3, equations (54)-(57) provide an excellent approximation to the behaviour of the full network, including the transition from tonic firing to bursting. Note that as the synaptic and adaptation time constants are biophysically derived, they cannot be made larger to satisfy the requirements of the quasi-steady state approximation. This is the major contributer the error in the mean-field equations, which we have confirmed via numerical solution of the PDE/ODE system (35)-(37). The error takes the form of shorter bursts then the actual network (see Figure 3(c)).

The simulations in Figure 3 display damped oscillations, indicative of an Andronov-Hopf bifurcation. Using the numerical continuation software MATCONT (Dhooge et al., 2003), we were able to determine that there is a subcritical-Andronov-Hopf bifurcation at $I = I_{AH}$. An unstable limit cycle emerges from this bifurcation for $I > I_{AH}$. This limit cycle corresponds to a spiking solution with periodically varying, nonzero firing rate. Using direct numerical simulations of the system of ODE's, we showed that the unstable limit cycle undergoes a grazing bifurcation with the switching manifold at $I = I_{GB}$, and becomes a non-smooth limit cycle for $I > I_{GB}$. Non-smooth limit cycles are limit cycles which cross the switching boundary. They correspond to bursting solutions in the full network. Shortly after, the unstable limit cycle collides with the stable non-smooth limit cycle in a saddle-node collision of limit cycles for some $I = I_{SNC} > I_{GB}$. Figure 4 contains the bifurcation diagram generated by a mixture of MATCONT and direct simulations of the full network, using I as the bifurcation parameter.

We can also determine the bifurcation manifolds numerically in the I, g_{syn} parameter space as shown in Figure 5. The parameters that correspond to bursting in the network lie below the curves shown in this figure, thus we will refer to this region in the parameter space as the "bursting region". For the mean field system, the Andronov-Hopf curves are computed in MATLAB by using a root finding package to determine the equilibrium values of $\langle w \rangle$ and s and then numerically evaluating the Jacobian. The curve where the full network transitions from tonic firing to bursting is determined as follows. A network of 1000 neurons and is simulated for 1000 ms over a 50×50 mesh in the parameter space. The variance in the interspike intervals is used to automatically classify the simulation for each mesh point as either bursting or tonically firing. A cubic spline is fit to the points that form the boundary between the two states. Initial conditions are chosen using a uniform distribution over $[v_{reset}, v_{peak}]$ for $v_i(0)$ and $s_i(0) = w_i(0) = 0,\ i = 1, \ldots, N$.

Note that the numerical continuation results for the mean field system show that for $I_{AH} < I < I_{SNC}$, the network displays bistability between the stable bursting limit cycle and the equilibrium point corresponding to tonic firing. Direct simulations of the network with varying initial conditions in s and w have verified this, as shown in Figure 6, although it appears that the network has a smaller region of bistability than the equations (54)-(57). Due to this bistability, it is difficult to accurately determine the bifurcation manifold associated with the transition to bursting via direct numerical simulations of the network. Despite this, and the other sources of error, the Andronov-Hopf manifold generated by the quasi-steady state approximation is still a good approximation to the boundary of the bursting region for the full network.

3.2 Example 2: An Excitatory Coupled Pair of Izhikevich Networks with Differing Adaptation Properties

Experimental work of Hemond et al. (2008) showed that pyramidal neurons in hippocampal area CA3 can be grouped into different populations based on the amount of spike frequency adaptation they exhibited, with 37% classified as strongly adapting and 46% as weakly adapting. The remainder were classified as intrinsically bursting. The work of Dur-e-Ahmad et al. (2012) and the previous section shows how the strength of adaptation in the single neuron relates to the existence of bursting in a homogeneous network. However, the biological network contains both weakly and strongly adapting neurons and in the work of Hemond et al. (2008) synaptic coupling was blocked, so the dominant firing pattern of this network is unknown. Thus it is of interest to study the firing patterns in a model of such a network. In this section we show how the techniques developed in this paper can be applied to this problem.

We consider a network consisting of two distinct, homogeneous populations, one which is strongly adapting and one which is weakly adapting. Since there are two populations, we require four maximal synaptic conductances g_{mj}, and two synaptic gating variables, s_j. Here j denotes the presynaptic network and m denotes the postsynaptic network, with $j = SA$ indicating the subnetwork with strong adaptation and $j = WA$ is the subnetwork with weak adaptation, and similarly for m. The equations for the network

are

$$C\dot{V}_{i,m} = k(V_{i,m} - V_T)(V_{i,m} - V_R) - W_{i,m} + I_{app,m} \tag{59}$$
$$+ (1-p)\, g_{syn,m\,SA}(E_r - V_{i,m})s_{SA} + p\, g_{syn,m\,WA}(E_r - V_{i,m})s_{WA}$$
$$\dot{W}_{i,m} = \frac{\eta(V_{i,m} - V_R) - W_{i,m}}{\tau_{W,m}} \tag{60}$$
$$\dot{s}_{SA} = -\frac{s_{SA}}{\tau_{syn}} + s_{jump} j_{SA}(t) \tag{61}$$
$$\dot{s}_{WA} = -\frac{s_{WA}}{\tau_{syn}} + s_{jump} j_{WA}(t) \tag{62}$$
$$j_{SA}(t) = \frac{1}{N_{SA}} \sum_{j=1}^{N_{SA}} \sum_{t_{j,k,SA}<t} \delta(t - t_{j,k,SA})$$
$$j_{WA}(t) = \frac{1}{N_{WA}} \sum_{j=1}^{N_{WA}} \sum_{t_{j,k,WA}<t} \delta(t - t_{j,k,WA})$$

for $i = 1, \dots N_m$, with the same discontinuities as the model in section 3.1. Here $p = N_{SA}/(N_{SA} + N_{WA})$ is the proportion of strongly adapting neurons in the network. The parameters can be found in Table 2. Aside from $g_{syn,mj}$ and $I_{app,m}$, the only other parameters that differ between the two populations are those that govern the adaptation levels, $\tau_{W,m}$ and $W_{jump,m}$.

After transforming equations (59)-(62) to dimensionless form, we can apply the ideas of the previous sections by considering the strongly adapting and weakly adapting populations to be described by their own distinct population density equation. The moment closure reduced population density equations are coupled together by the two coupling variables, two adaptation variables and the following fluxes:

$$J_{SA}(v) = \rho_{SA}(v)(v(v-\alpha) - \langle w\rangle_{SA} + I_{SA} + (1-p)\, g_{SA,SA}(e_r - v)s_{SA,SA} + p\, g_{SA,WA}(e_r - v)s_{SA,WA})$$
$$J_{WA}(v) = \rho_{WA}(v)(v(v-\alpha) - \langle w\rangle_{WA} + I_{WA} + p\, g_{WA,SA}(e_r - v)s_{WA,SA} + (1-p)\, g_{WA,WA}(e_r - v)s_{WA,WA}).$$

Applying the quasi-steady state approximation, as before, the resulting system of ordinary differential equations is:

$$\langle w\rangle'_{SA} = -a_{SA}\langle w\rangle + w_{jump,SA}\langle R_i(t)\rangle_{SA} \tag{63}$$
$$\langle w\rangle'_{WA} = -a_{WA}\langle w\rangle + w_{jump,WA}\langle R_i(t)\rangle_{WA} \tag{64}$$
$$s'_{SA} = -\frac{s_{SA}}{\tau_s} + s_{jump}\langle R_i(t)\rangle_{SA} \tag{65}$$
$$s'_{WA} = -\frac{s_{WA}}{\tau_s} + s_{jump}\langle R_i(t)\rangle_{WA}. \tag{66}$$

Here we have :

$$\langle R_i(t)\rangle_{SA} = \begin{cases} \left(\int_V \frac{dv}{v(v-\alpha) - \langle w\rangle + I_{SA} + g_{SA,WA}(e_r - v)s_{WA} + g_{SA,SA}(e_r - v)s_{SA}} \right)^{-1}, & I_{SA} \geq I^*_{SA} \\ 0 & I_{SA} < I^*_{SA} \end{cases} \tag{67}$$

and

$$I^*_{SA}(\langle w\rangle_{SA}, s_{SA}, s_{WA}) = \langle w\rangle_{SA} + \frac{(\alpha + g_{SA,SA}s_{SA} + g_{SA,WA}s_{WA})^2}{4} \tag{68}$$

$$- e_r(g_{SA,SA}s_{SA} + g_{SA,WA}s_{WA}), \tag{69}$$

with a similar equation holding for $\langle R_i(t)\rangle_{WA}$. As in numerical example 1, each $\langle R_i(t)\rangle_m$ can be evaluated explicitly and is a slight modification of $\langle R_i(t)\rangle$ for numerical example 1. These explicit expressions are used in the numerical studies. Note that the dimensionless parameters, I_m, g_{mj} etc have the same scaling as shown in Table 1.

The mean field model is accurate quantitatively and qualitatively in the tonic firing (Figure 7) and bursting (Figure 8) regimes. Note that in the "bursting" state, only the strongly adapting population bursts, while the weakly adapting population has an oscillatory firing rate that peaks in synchrony with the bursts in the strongly adapting population.

For this type of network we find a very similar bifurcation diagram to that of the single network of strongly adapting Izhikevich neurons studied in numerical example 1. The bifurcation sequence consists of a subcritical Andronov-Hopf bifurcation followed by a grazing bifurcation and a saddle-node collision of limit cycles, as shown in Figure 9. However, the size of the bursting region depends on the relative sizes of the two populations. To allow for a direct comparison, we use as our bifurcation parameters $I_{app,SA}$ and $g_{syn,SA,SA}$ and fix all the other parameters at the values in Table 2. Direct simulations are run over a mesh and compared to the bifurcations of the system (63)-(66). The Andronov-Hopf manifold for the ODE's is solved for numerically in MATLAB, as described in example 1. Once again we can conclude that the mean field system of switching ODE's is an adequate quantitative and qualitative descriptor of the behavior of the full network.

Figure 10 shows the results of a series of simulations where the proportion, p, of strongly adapting neurons in the network is varied. The network consists of 1000 neurons with $N_{SA} = 1000p$ strongly adapting and $N_{WA} = 1000(1-p)$ weakly adapting. The boundary of the bursting region was computed for the mean field model and the full network as described in the previous subsection. For a higher proportion, this boundary is shifted into the low synaptic conductance region, while for a lower proportion, the manifold is shifted to

$W_{jump,SA}$	200 pA
$W_{jump,WA}$	100 pA
$\tau_{W,SA}$	100 ms
$\tau_{W,WA}$	10 ms
$I_{app,SA}$	1000-2000 pA
$I_{app,WA}$	1200 pA
$g_{syn,mj}$	200 nS
N_{SA}	800
N_{WA}	200

Table 2: Parameters for the two coupled Izhikevich networks in numerical example 2. All parameters that are not mentioned in this table can be found in Table 1. These parameters apply unless otherwise indicated.

the high synaptic conductance region. Not surprisingly, we can conclude that networks with more weakly adapting neurons stabilize the tonic firing behavior of the full network for smaller synaptic conductances. The mean field model seems to be a worse approximation of the full network when the proportion of weakly adapting neurons is low. This may be due to the fact for these neurons, the perturbation approximation ($b = 0$) is not as accurate.

3.3 Example 3: A Coupled Pair of Adaptive Exponential Networks with Excitation and Inhibition

The parameters for an AdEx neuron have recently been fitted to both excitatory and inhibitory cortical neurons (Naud et al., 2008). We use these parameters to simulate a coupled network consisting of a population of inhibitory neurons and one of excitatory neurons. The equations for the network are:

$$C_m \dot{V}_{i,m} = -g_{L,m}(V_{i,m} - E_{L,m}) + g_{L,m} \exp\left(\frac{V_{i,m} - V_{T,m}}{\Delta_{T,m}}\right) - W_{i,m} + I_m + \sum_k p_k g_{mk}(V_{i,m} - E_{R,k}) s_k \tag{70}$$

$$\dot{W}_{i,m} = a\left(b\left(V_{i,m} - E_{L,m}\right) - W_{i,m}\right) \tag{71}$$

$$\dot{s}_k = -\frac{s_k}{\tau_{R,k}} + h_k \tag{72}$$

$$\dot{h}_k = -\frac{h_k}{\tau_{D,k}} + \frac{1}{\tau_{R,k}\,\tau_{D,k}} j_k(t), \tag{73}$$

where $i = 1, 2 \ldots N_m$ and $p_k = N_k/(N_I + N_E)$. Here $m, k = E$ for the excitatory network, and $m, k = I$ for the inhibitory network. Note that this model incorporates double exponential synapses. The parameters for

this model are given in Table 3. Following Markram et al. (2004), we assume that the network consists of 80% excitatory neurons and 20% inhibitory neurons.

The reduction procedure for this model is similar to that for the example 2. Without nondimensionalizing the equations, we define a population density equation for each population. The reason for not applying the nondimensionalization is that applying it to populations with two completely different parameter sets results in a messier system of equations. The non-dimensional equations and the dimensional equations remain equivalent however. With that in mind, the quasi-steady state approximation is then applied to both population density equations, yielding a system of six autonomous, switching ODE's:

$$s_I{}' = -\frac{s_I}{\tau_{R,I}} + h_I \tag{74}$$

$$h_I{}' = -\frac{h_I}{\tau_{D,I}} + \frac{\langle R_i(t)\rangle_I}{\tau_{R,I}\tau_{D,I}} \tag{75}$$

$$s_E{}' = -\frac{s_E}{\tau_{R,E}} + h_E \tag{76}$$

$$h_E{}' = -\frac{h_E}{\tau_{D,E}} + \frac{\langle R_i(t)\rangle_E}{\tau_{R,E}\tau_{D,E}} \tag{77}$$

$$\langle w\rangle_E' = -\frac{\langle w\rangle_E}{\tau_{W,E}} + w_{jump,E}\langle R_i(t)\rangle_E \tag{78}$$

$$\langle w\rangle_I' = -\frac{\langle w\rangle_I}{\tau_{W,I}} + w_{jump,I}\langle R_i(t)\rangle_I, \tag{79}$$

where the firing rates are given by

$$\langle R_i(t)\rangle_m = \begin{cases} \left[\int_V \frac{C_m\, dv}{-g_{L,m}(V_{i,m}-E_{L,m}) + g_{L,m}\exp\left(\frac{V_{i,m}-V_{T,m}}{\Delta_{T,m}}\right) - \langle w\rangle_m + I_m + \sum_k p_k g_{mk}(V_{i,m}-E_{R,k})s_k}\right]^{-1} & , I_m \geq I_m^* \\ 0 & I_m < I_m^* \end{cases}$$

The integrals cannot be evaluated explicitly, thus they are evaluated numerically using the trapezoidal method. The equations for the switching manifold are somewhat lengthy, but they can be easily derived merely by evaluating v' at the point

$$v_m^* = V_{T,m} + \Delta_{T,m}\log\left(1 + \frac{\sum_k p_k g_{mk} s_k}{g_{L,m}}\right),$$

and subsequently solving for $I_m = I^*(s_E, s_I, \langle w\rangle_m)$.

We begin by removing the synaptic coupling within each population ($g_{EE} = g_{II} = 0$) for the sake of simplicity and for the purpose of eliminating the adaptation induced bifurcation seen in the previous two numerical examples. In this case, the switching manifolds only depend on one of the gating variables. For example, the excitatory population switching manifold is $I_E = I^*(s_I, \langle w\rangle_E)$. Comparisons of the behaviour of the mean field model and the full network are given in Figures 11 and 12. Corresponding voltage traces

C_E	104 pF	C_I	59 pF
$g_{L,E}$	4.3 nS	$g_{L,I}$	1.7 nS
$E_{L,E}$	-65 mV	$E_{L,I}$	-62 mV
$V_{T,E}$	-52 mV	$V_{T,I}$	-42 mV
$\Delta_{T,E}$	0.8 mV	$\Delta_{T,I}$	3.0 mV
I_E	1000 pA	I_I	100 pA
$\tau_{1,E}$	0.1 ms	$\tau_{1,I}$	1 ms
$\tau_{2,E}$	2 ms	$\tau_{2,I}$	20 ms
a_E	0.01 $(\text{ms})^{-1}$	a_I	0.1 $(\text{ms})^{-1}$
b_E	-0.8 nS	b_I	2.0 nS
$V_{peak,E}$	0 mV	$V_{peak,I}$	0 mV
$V_{reset,E}$	-53 mV	$V_{reset,I}$	-54 mV
$W_{jump,E}$	200 pA	$W_{jump,I}$	50 pA
$E_{R,E}$	-25 mV	$E_{R,I}$	-50 mV
N_E	800	N_I	200

Table 3: Parameters (from Naud et al. (2008)) for the two coupled AdEx networks in numerical example 3. These parameters apply unless otherwise indicated.

of random neurons from the network are shown in Figure 13 (a) and (b). In Figure 11, the mean field model indicates the system is tonically firing. However Figures 11 and 13(a) indicate the full network is in a mixed state, with the excitatory population tonically firing and the inhibitory population bursting. In Figure 12, the mean field model indicates the system has an oscillatory firing rate, while Figures 12 and 13(b) indicate the full system is in a bursting state. We have also used numerical continuation to study the bifurcations of the mean field model and found that there is not a good correspondence with the bifurcations of the full network.

If we consider nonzero recurrent synaptic coupling ($g_{EE}, g_{II} \neq 0$), other interesting oscillatory firing rates can occur. For example, in one parameter regime, multi-phase bursts appear. In this firing regime, the excitatory network fires regular bursts, while the inhibitory network fires a two-phase burst, as shown in Figure 13(c). The mean field model replicates these multi-phase bursts both quantitatively and qualitatively (Figure 14).

For the E/I AdEx network, whether or not the mean field model adequately represents behaviour of the full network is parameter dependent. A possible reason for the poor approximation of the mean field model

is that the network is synchronized in the examples above. It is known that mean field approximations may not be valid in this case (Nesse et al., 2008).

4 Discussion

Starting from a population density equation, we rigorously derived a mean field approximation to a large network of two-dimensional neurons based on a separation of time scales. We then applied the resulting switching ODE's to different examples of large networks where the forces of inhibition, adaptation, and excitation interact. The differential equations were used to determine bifurcation manifolds and types for the networks in question. Such bifurcation studies can be in turn used to make predictions about the biological networks being studied as we illustrate below.

One of the striking features of networks of neurons in area CA3 is their tendency to burst. However, experimental data shows that when all synaptic input is blocked, only a minority of the neurons in the CA3b region of the hippocampus are observed to be intrinsically bursting (Hemond et al., 2008). The majority can be grouped into strongly adapting and weakly adapting subpopulations (Hemond et al., 2008). In section 3.2 we proposed a model which is an extension of that of Dur-e-Ahmad et al. (2012) to a network which contains both weakly and strongly adapting neurons. The mean-field model we derived, (63)-(66), allowed us to compute the bifurcation manifolds for an all-to-all coupled network with various proportions of strongly and weakly adapting neurons.

Based on the work of Ho et al. (2009), we can estimate biologically relevant ranges of g_{syn} to be on the order of 10's of nS, which is on the lower side of the bursting region diagrams (Figures 5 and 10). We note that these synaptic values from Ho et al are estimated during spontaneously generated population activities in CA3 networks. As such, they are the most directly applicable measurements to aid in the interpretation of our bifurcation diagrams.

Given the biological constraints on the magnitude of the synaptic conductance, we can predict how an actual network of neurons would behave. The analysis of section 3.1 (see Figure 5) predicts that for currents just over rheobase, a network composed entirely of strongly adapting neurons will burst, confirming the analysis of Dur-e-Ahmad et al. (2012). However, once weakly adapting neurons are added, the intersection of the bifurcation manifold with the rheobase current shifts toward the right for increasing proportions of weakly adapting neurons (see Figure 10). In fact, only for networks where a majority of neurons are strongly

adapting does the network have a bursting region inside the biologically reasonable range of conductance values. However, estimates from actual CA3 pyramidal cells indicate that 37% of the neurons were strongly adapting and 46% were weakly adapting, with the remaining 16% being intrinsically bursting (Hemond et al., 2008). Our results indicate that a network with this proportion of strongly to weakly adapting neurons would be tonically firing. This means that something more is needed in the model to obtain the bursting seen experimentally. One possibility is that the small proportion of intrinsically bursting neurons is critical for network bursting. Adaptation may thus only facilitate rhythmic bursting in the networks, while a small subset of intrinsically bursting neurons acts as the spark to start the rest of the network. A mean-field approach with the addition of an intrinsically bursting subpopulation of Izhikevich neurons would allow us to determine if the bifurcation region expands outward to low conductance values. Exploring this hypothesis further is an area for future work.

4.1 Sources of Error

The validity of our mean field approximation is based on a series of assumptions/requirements that are imposed during the derivation. We list them in order of appearance

1. $\langle w|v\rangle = \langle w\rangle$ (First order moment closure method, fast firing rates)
2. $\langle w\rangle \gg w_{jump}$ (Mean adaptation is much greater then individual jump sizes.)
3. $b \ll O(1)$ (Perturbation arguement to decouple $\langle w\rangle$ from $\langle v\rangle$.)
4. $\tau_s, \tau_w \gg O(1)$ (Quasi-steady state approximation)
5. $\langle R_i(t)\rangle = 0$ if $I \leq I^*(s, \langle w\rangle)$. (The residual firing rate past the switching manifold is negligible.)

Of these five requirements, only the fourth is truly indispensible. Without it, the quasi-steady state approximation is no longer valid. However, even when τ_s and τ_w are only moderately larger then 1, the approximation is still fairly good. For example, in numerical example 1, $\tau_s = 2$ ms and the accuracy of the approximation in that example is still satisfactory. However, it is simply not possible to eliminate this as a source of error for biophysically derived time constants that are not large. The application of this approach should be limited to those cases as we have numerically found the quasi-steady state approximation to be the largest contribution to the error in the mean-field equations when the conditions on the time constants are not satisfied. The other four requirements for applicability of this approach may be dealt with in different ways.

One way to improve on the first order moment closure assumption is to use a higher order moment closure method (Ly and Tranchina, 2007). That is, to use the approach of section 2.2, but approximate the kth conditioned moment as a linear combination of the first $k-1$ conditioned moments, and the first k unconditioned moments. It is unclear whether or not such a higher order moment closure method, when used in conjunction with the quasi-steady state approximation, would yield a greater degree of accuracy than the lowest order method. Investigation of this is an area for future work.

We used the second assumption to justify dropping the $O(w_{jump}^2)$ terms in the equation for $\langle w \rangle'$. This approximation may be improved by trying to estimate the higher order terms in the Taylor expansion in equation (31).

The perturbation argument was used to eliminate the term involving the unknown $\langle v \rangle$. However, when the quasi-steady state approximation is used it is possible to compute $\langle v \rangle$ (and thus not employ the perturbation argument) via the relationship

$$\langle v \rangle = \int_V \frac{v J(s, \langle w \rangle), dv}{F(v) - w + I + gs(e_r - v)}. \tag{80}$$

This will result in an extra term in equation for $\langle w \rangle'$ (equation (44)). We have computed this in the case that $b \ll 1$ to verify that the perturbation argument is valid. Note that (80) is only valid for $I > I^*(s, \langle w \rangle)$, since for $I \leq I^*(s, \langle w \rangle)$, the the quasi-steady state approximation breaks down as discussed in section 2.3.

As discussed in section 2.3, when $I = I^*(s, \langle w \rangle)$, the emergence of fixed points in equation (40) causes the flux to change direction in different regions of the phase space of v, which means the quasi-steady state assumption $\frac{\partial J}{\partial v} = 0$ breaks down. This breakdown makes it difficult to compute the residual firing rates for $I \leq I^*(s, \langle w \rangle)$. However, we have found this contribution to be small and not worth the added effort required to determine the residual firing rate.

4.2 Comparison with Other Mean-Field Equations

Seldom is a mean-field system of equations analytically derivable from the original network equations. However, it has been done in the literature for a few cases, which we now describe and compare with our work.

Nesse et al. (2008) derived mean-field equations for networks of fully coupled, linear integrate and fire neurons containing synaptically filtered noise and two different models for adaptation. The structure of

the equations derived is the same as ours, consisting of a closed system of non-smooth ordinary differential equations for the moments of the adaptation and synaptic variables. While their networks are stochastic, and they use different adaptation model than us, they derive a similar equation for the mean-adaptation for one of their networks (Equations (25)-(26) in Nesse et al. (2008)). Additionally, we have verified that if the stochastic inputs are removed from their model and our derivation is used, the same mean-field systems for both kinds of adaptation will result. Note, however, that the interpretation of the network averaged firing rate, $\langle R_i \rangle$, changes between the deterministic and stochastic network.

La Camera et al. (2004, 2008) derived mean-field equations for an uncoupled network of linear integrate and fire neurons with the same adaptation model as us and containing synaptically filtered noise. The mean adaptation equations presented by La Camera et al. (2004, 2008) are the same as our differential equation for the first moment of the adaptation current w in our networks (compare Equation (44) with Equation (3.3) in La Camera et al. (2004)). Again, there is a different interpretation of what the network averaged firing rate is under the case of noise. We note that it should be possible to derive precisely the same set of equations as in La Camera et al. (2004) for our network of two-dimensional neurons with synaptically filtered noise, by using the first order moment-closure and quasi-steady state approximations together, in conjunction with a diffusion approximation. In fact, the first order moment closure approximation may be better under cases of low firing rates when one adds noise. The reason for this is that adding noise to the voltage variable of a neuron (either synaptically filtered or otherwise) should decouple it from the adaptation variable.

Vladimirski et al. (2008) have derived mean field equations for a network of linear integrate and fire neurons with synaptic depression and input currents which are either heterogeneous and deterministic or homogeneous and noisy. For the heterogeneous network, they note that one cannot use a single variable for the average depression to predict the behavior of the network. However, for their homogeneous network, they derive a mean-field equation for their mean synaptic depression, in terms of their network averaged firing rate (Equation (17),Vladimirski et al. (2008)). This equation is analogous to the equation for the mean adaptation variable in our model and those described above. Unlike our mean-field model and that of Nesse et al. (2008), the mean-field model of Vladimirski et al. (2008) has no differential equation for the mean synaptic gating variable. They use a time scale separation argument to derive an expression for the average of this variable over one oscillation period. This is equivalent to applying a quasi-steady state approximation

to the equation for s in our model. Further, since Vladimirski et al. (2008) represent depression using a kinetic model Destexhe et al. (1998) the derivation of the mean field equation is done by time averaging the fast gating variable over an oscillation period, as opposed to the approach used by Nesse et al. (2008); La Camera et al. (2004, 2008) and us. Finally, Vladimirski et al. (2008) note that adaptation and depression work through two different mechanisms, yet both can yield rhythmic bursting. It would be interesting to derive the mean-field system for both depressing and adapting two-dimensional networks and compare how these two mechanisms differ analytically.

4.3 Extending the Technique to More Realistic Networks

A natural extension to consider is to networks of conductance based neurons. The primary difficulty in applying the theory to this situation is determining the relationship between the flux and the firing rate. Since neuron firing in conductance based models is not caused by a reset but occurs through a natural oscillation, the discussion of section 2 and the appendix does not apply. A natural first case to consider is simple two dimensional oscillator such as the Fitzhugh-Nagumo model (Fitzhugh, 1952). Once this is overcome in a simple two-dimensional model, it should be possible to extend the theory to more realistic conductance based models.

To further the applicability of this approach, more realistic network topologies should be considered. Seldom are networks of neurons all-to-all coupled in the real world. The networks are often sparsely connected, with the level of sparsity possibly acting as a bifurcation parameter itself. Fortunately, Omurtag et al. (2000) have developed some extensions of population density methods to networks of linear integrate and fire neurons with sparse coupling. Preliminary work we have carried out indicates that these extensions should be applicable to higher dimensional neurons.

Furthermore, kinetic modeling of synapses, as pioneered by Destexhe et al. (1998), is the most biologically plausible approach to modeling the synaptic interaction between neurons. The kinds of synapses we have considered do not fall into this class. Thus, the technique will need to be extended to these more realistic models of synaptic dynamics. It will be interesting to compare this approach to that used be Vladimirski et al. (2008) to deal with kinetically modelled variables.

Appendix

Relationship Between the Flux and the Firing Rate

Here we show that in the limit that $N \to \infty$, the quantity

$$j(t) = \frac{1}{N} \sum_{j=1}^{N} \sum_{t_{j,k}<t} \delta(t - t_{j,k}) \tag{81}$$

converges to the network averaged instantaneous firing rate. We then relate this firing rate to a flux described in section 2.1. We will think of $j(t)$ and its limit as distributions.

Note that one needs to be careful in defining a mean or average firing rate, as there are at least three definitions in the literature. See Gerstner and Kistler (2002) for a good discussion of this. To define the appropriate rate for our purposes, we first define the function $n_i(t)$ to be the number of spikes fired by the ith neuron in the time interval $[0, t]$. One can then relate $j(t)$ to the average of $\langle n_i(t) \rangle$ across the network:

$$\langle n_i(t) \rangle = \lim_{N\to\infty} \frac{1}{N} \sum_{i=1}^{N} \int_0^t \sum_{t_{i,k}<t} \delta(x - t_{i,k})\, dx = \lim_{N\to\infty} \int_0^t j(x)\, dx. \tag{82}$$

Then we define $\langle R_i(t) \rangle$ as

$$\langle R_i(t) \rangle = \lim_{\Delta t\to 0} \frac{1}{\Delta t} \lim_{N\to\infty} \frac{1}{N} \sum_{i=1}^{N} \frac{n_i(t + \Delta t) - n_i(t)}{N}. \tag{83}$$

Thus, the network averaged firing rate in this sense is the limit of the population activity as $\Delta t \to 0$. However, rearranging the limits, this may also be written

$$\langle R_i(t) \rangle = \lim_{\Delta t\to 0} \frac{\langle n_i(t + \Delta t) \rangle - \langle n_i(t) \rangle}{\Delta t} = \frac{d}{dt} \langle n_i(t) \rangle. \tag{84}$$

Thus, in the limit $N \to \infty$, we can replace $j(t)$ in the synaptic coupling equation with $\langle R_i(t) \rangle$.

Now, all that remains is to relate the firing rate to the flux. For the integrate and fire models we are considering, there is a surface $\mathcal{F} = 0$ which defines when a neuron has fired. As the flux is a kind of directional flow rate of the proportion of neurons at a particular point in phase space, the firing rate can be computed by integrating the flux vector over this "firing boundary":

$$\langle R_i(t) \rangle = \int_{\mathcal{F}} \mathbf{J} \cdot \mathbf{n}\, dS,$$

where $\mathbf{n}$ is the outward normal to the firing boundary. For example, the flux for a system of one dimensional neurons, $J(v, t)$ is merely the proportion of neurons that flow across the point v in phase space per unit time at time t. Now for a network of linear integrate and fire neurons the firing boundary is the point $v = v_t$ in the v phase space, thus the firing rate is $J(v_t, s, t)$, the flux through the threshold. For the class of neurons we are dealing with, however, the firing boundary is given by the line $v = v_{peak}$ in the v, w phase space. Thus the surface integral reduces to integrating the v component of the flux, evaluated at $v = v_{peak}$, over the entire range of w in phase space:

$$\langle R_i(t) \rangle = \int_W J_V(v_{peak}, w, s, t)\, dw. \tag{85}$$

Acknowledgements This work benefitted from the support of the Natural Sciences and Engineering Research Council of Canada and the Ontario Graduate Scholarship program. The authors would like to thank F. Skinner for useful discussions. The authors would also like to thank the reviewers for their suggestions which improved the manuscript.

References

Abbott, L.F. & van Vreeswijk, C. (1993) Asynchronous states in networks of pulse-coupled oscillators. Learning and Memory 48(2):1483–1490

Apfaltrer, F., Ly, C., & Tranchina, D. (006) Population density methods for stochastic neurons with realistic synaptic kinetics: Firing rate dynamics and fast computational methods. Network: Computation in Neural Systems 17(4):373–418

di Bernardo, M., Budd, C., Champneys, A., Kowalczyk, P., Nordmark, A., Tost, G., & Piiroinen, P. (2008) Bifurcations in non-smooth dynamical systems. SIAM Review 50(4):629–701

Brette, R. & Gerstner, W. (2005) Adaptive exponential integrate-and-fire model as an effective description of neuronal activity. Journal of Neurophysiology 94(5):3637–3642

Casti, A., Omurtag, A., Sornborger, A., Kaplan, E., Knight, B.W., Victor, J., & Sirovich, L. (2002) A population study of integrate-and-fire-or-burst neurons. Neural Computation 14(5):957–986

Destexhe A., Mainen Z., & Sejnowski, T. (1998) Kinetic models of synaptic transmission. In: Koch C, Segev I (eds) Methods in Neuronal Modeling: From Synapses to Networks, MIT Press, Cambridge, MA, chap 1

Dhooge A., Govaerts W., & Kuznetsov, Y.A. (2003) MatCont: A MATLAB package for numerical bifurcation analysis of ODEs. ACM Transactions on Mathematical Software 29:141–164

Dur-e-Ahmad, M., Nicola, W., Campbell, S.A., & Skinner, F. (2012) Network bursting using experimentally constrained single compartment CA3 hippocampal neuron models with adaptation. Journal of Computational Neuroscience 33(1):21–40

Ermentrout, G.B. & Terman, D.H. (2010) Mathematical Foundations of Neuroscience. Springer, New York, NY

Fitzhugh, R. (1952) Impulses and phsyiological states in theoretical models of nerve membrane. Biophysical J 1(6):445–466

Gerstner, W., & Kistler, W. (2002) Spiking Neuron Models. Cambridge University Press

Hines, M.L., Morse, T., Migliore, M., Carnevale, N.T., Shepherd, G.M. ModelDB: A database to support computational neuroscience. J Comput Neurosci. 2004 Jul-Aug;17(1):7-11.

Hemond, P., Epstein, D., Boley, A., Migliore, M., Ascoli, G., & Jaffe, D. (2008) Distinct classes of pyramidal cells exhibit mutually exclusive firing patterns in hippocampal area CA3b. Hippocampus 18(4):411–424

Ho, E.C., Zhang, L., & Skinner, F.K. (2009) Inhibition dominates in shaping network activities in vitro. Hippocampus 19(2):152–165

Izhikevich, E. (2003) Simple model of spiking neurons. Neural Networks, IEEE Transactions on 14(6):1569 – 1572

Knight, B.W. (2000) Dynamics of encoding in neuron populations: Some general mathematical features. Neural Computation 12:473–518

La Camera, G., Rauch, A., Luscher, H.R., Senn, W., & Fusi, S. (2004) Minimal models of adapted neuronal response to in-vivo like input currents. Neural Computation 16:2101–2124

La Camera, G., Giugliano, M., Senn, W., & Fusi, S. (2008) The response fo cortical neurons to in vivo-like input current: theory and experiment, Biological Cybernetics 99:279–301

Ly, C., & Tranchina, D. (2007) A critical analysis of dimension reduction by a moment closure method in a population density approach to neural network modeling. Neural Computation 19(8):2032–2092

Markram H., Toledo-Rodriguez M., Wang Y., Gupta A., Silberberg G., Wu C. (2004) Interneurons of the neocortical inhibitory system. Nature Reviews: Neuroscience 5(10):793–807

MATLAB (2012) version 7.10.0 (R2012a). The MathWorks Inc., Natick, Massachusetts

Naud R., Marcille N., Clopath C., Gerstner W. (2008) Firing patterns in the adaptive exponential integrate-and-fire model. Biological Cybernetics 99:335–347

Nesse W., Borisyuk A., Bressloff P. (2008) Fluctuation-driven rhythmogenesis in an excitatory neuronal network with slow adaptation. Journal of Computational Neuroscience 25:317–333, 10.1007/s10827-008-0081-y

Nykamp D., Tranchina D. (2000) A population density approach that facilitates large-scale modeling of neural networks: Analysis and an application to orientation tuning. Journal of Computational Neuroscience 8:19–50

Omurtag A., Knight B.W., Sirovich L. (2000) On the simulation of large populations of neurons. Journal of Computational Neuroscience 8:51–63

Sirovich L., Omurtag A., Knight B.W. (2000) Dynamics of neuronal populations: The equilibrium solution. SIAM Journal on Applied Mathematics 60(6):pp. 2009–2028

Sirovich L., Omurtag A., Lubliner K. (2006) Dynamics of neural populations: Stability and synchrony. Network: Computation in Neural Systems 17:3–29

Strogatz S., Mirollo R.E. (1991) Stability of incoherence in a population of coupled oscillators. Journal of Statistical Physics 63:613–635

Tikhonov A. (1952) Systems of differential equations containing small parameters in the derivatives (in Russian). Matematicheskii Sbornik (NS) 31(73):575–586

Touboul J. (2008) Bifurcation analysis of a general class of nonlinear integrate-and-fire neurons. SIAM Journal on Applied Mathematics 68(4):1045–1079

Treves A. (1993) Mean-field analysis of neuronal spike dynamics. Network: Computation in Neural Systems 4(3):259–284

van Vreeswijk C. (1996) Partial synchronization in populations of pulse-coupled oscillators. Physical Review E 54:5522–5537, DOI 10.1103/PhysRevE.54.5522

van Vreeswijk C., Hansel D. (2001) Patterns of synchrony in neural networks with spike adaptation. Neural Computation 13(5):959–992

van Vreeswijk C., Abbott L.F., Ermentrout G.B. (1994) When inhibition not excitation synchronizes neural firing. Journal of Computational Neuroscience 1:313–321

Vladimirski, B.B., Tabak, J., O'Donovan, M.J., Rinzel J. (2008) Episodic acitivty in a heterogeneous excitatory network, from spiking neurons to mean field. Journal of Computational Neuroscience 25:39–63

Wu Y., Lu, W., Lin, W., Leng, G., Feng, J. (2012) Bifurcations of Emergent Bursting in a Neuronal Network. PLoS ONE 7(6):e38402.

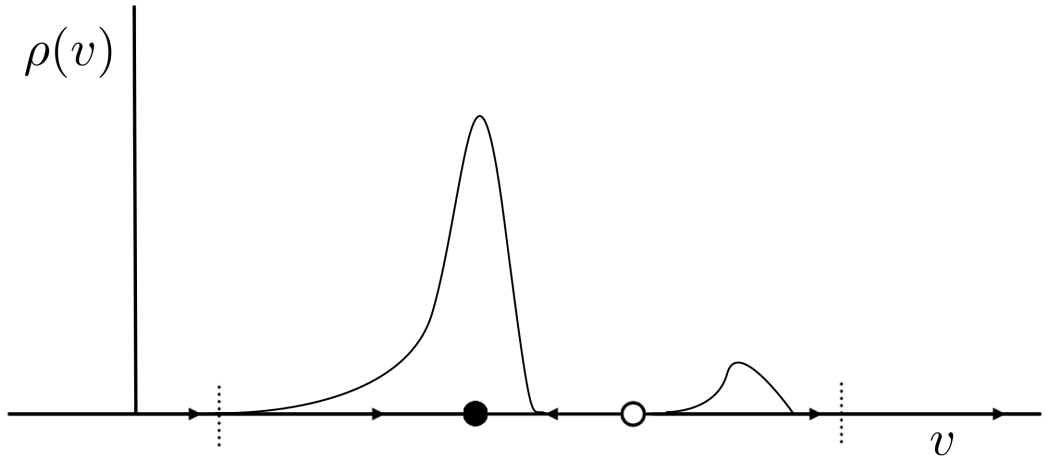

Fig. 1: The saddle-node bifurcation of the mean neuron equation (40) results in two fixed points. Note that these fixed points only exist in the mean sense. The stable point attracts density within its basin of attraction and its peak becomes increasingly sharp. The unstable node repels density towards the stable node either directly, or indirectly through v_{peak}. Density that leaves through v_{peak} is reabsorbed through v_{reset} and then lies within the basin of attraction of the stable node. This means there is a residual firing rate, i.e., $\langle R_i(t)\rangle \neq 0$ when $I \leq I^*(\langle w\rangle, s)$.

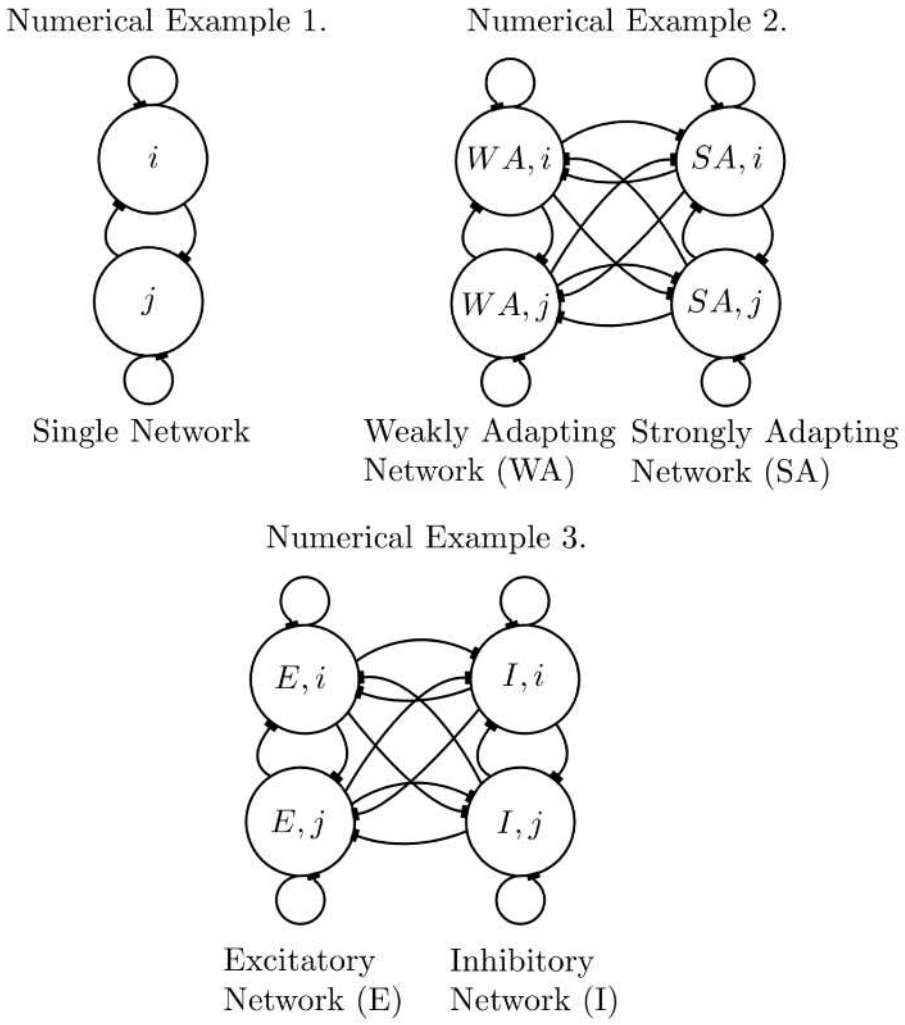

Fig. 2: The network topology for the three numerical examples studied in this paper. Numerical example 1 is an all-to-all coupled network of Izhikevich neurons. Numerical example 2 consists of two all-to-all cross coupled networks of Izhikevich neurons. One of them is weakly adapting, and the other is strongly adapting. Numerical example 3 consists of two cross-coupled networks of AdEx neurons. One network is inhibitory, while the other is excitatory.

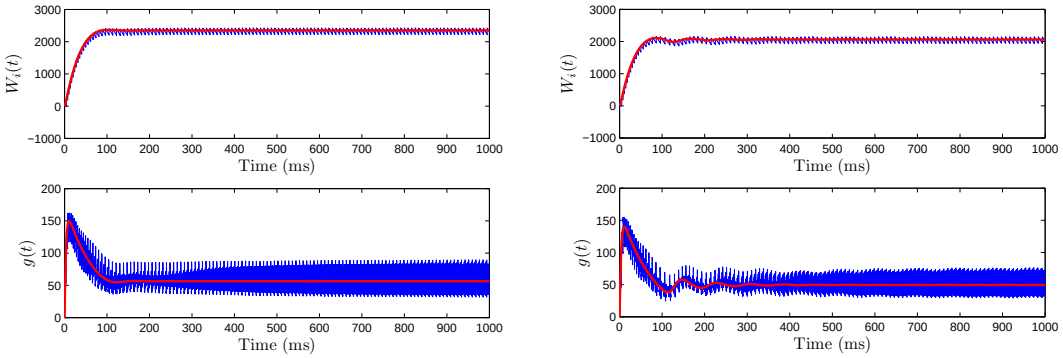

(a) $I_{app} = 2500$ pA

(b) $I_{app} = 2200$ pA

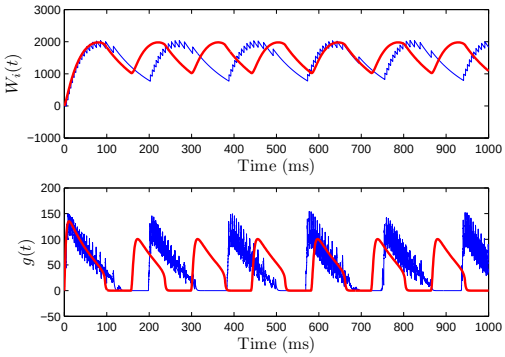

(c) $I_{app} = 2050$ pA

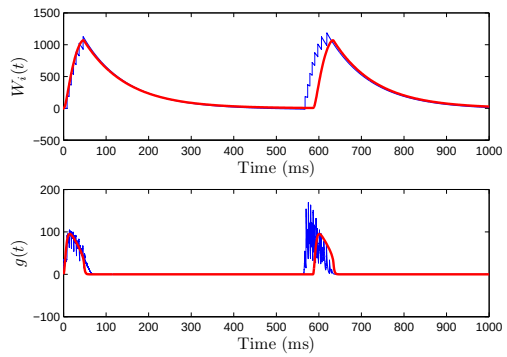

(d) $I_{app} = 1025$ pA

Fig. 3: Comparison of behaviour from numerical simulation of a network of 1000 Izhikevich neurons (46)-(49) and of the corresponding mean field model (54)-(57). Show in blue are the network average synaptic conductance, $g(t)$, and the adaptation current of a random neuron, $W(t)$, from the full network. Shown in red are the corresponding variables in the mean field model, $g_{syn}s(t)$ and $\langle w \rangle$. I_{app} varies from panel to panel as shown while $g_{syn} = 300$ nS for every panel. The rest of the parameter values can be found in Table 1.

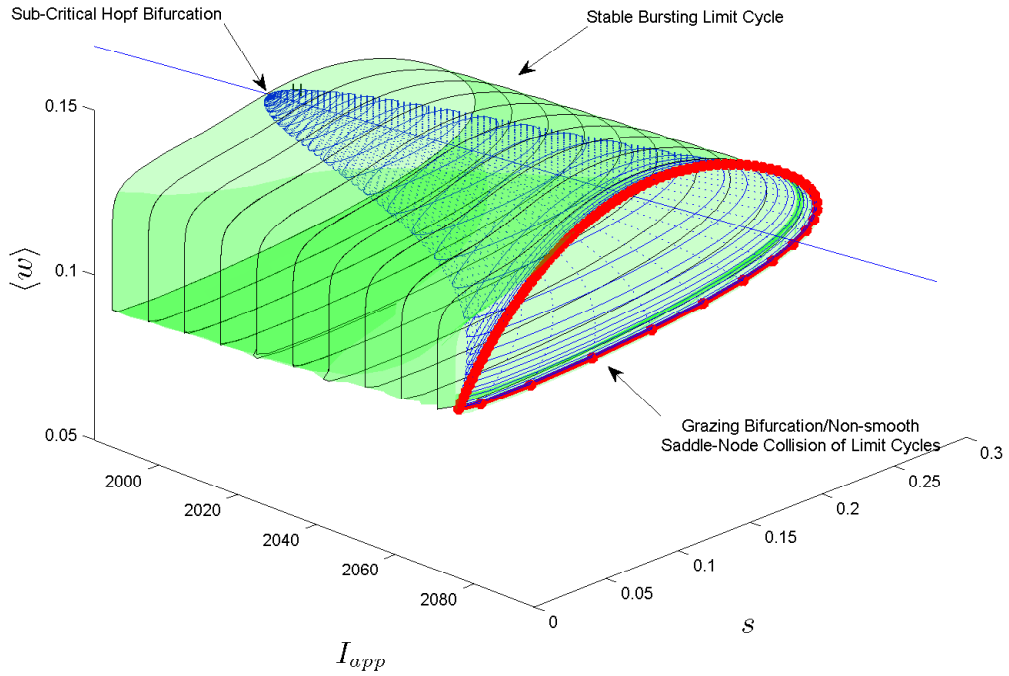

Fig. 4: A combination of numerical simulation and numerical continuation determines the bifurcations that occur in the mean field model (54)-(57). The parameters can be found in Table 1. A subcritical Hopf bifurcation occurs at $I_{app} \approx 1983$ pA which causes the emergence of a unstable limit cycle. As I_{app} is increased, the unstable limit cycle grows in amplitude (blue surface), eventually touching the switching manifold in a grazing bifurcation at $I_{app} = I_{GB}$ (red curve) and becomes a non-smooth limit cycle, which corresponds to bursting (green surface) in the full network. For a narrow region past the grazing bifurcation, the unstable limit cycle persists, eventually colliding with the stable non-smooth limit cycle at $I_{app} \approx 2075$ pA (not shown, near red curve). The equilibrium point corresponding to tonic firing is stable for $I_{app} > 1983$ and unstable otherwise.

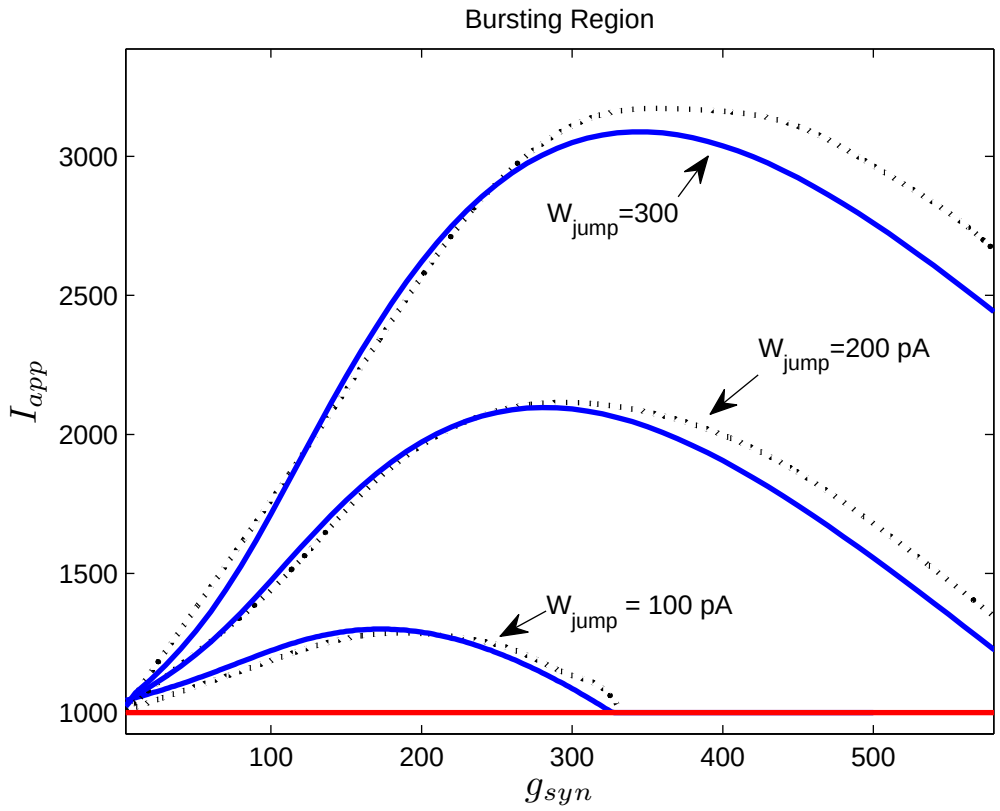

Fig. 5: The bifurcation manifolds associated with the transition from tonic firing to bursting for three different W_{jump} values. Larger W_{jump} corresponds to stronger adaptation in the neural model. The Hopf manifold for the reduced system (54)-(57), calculated using numerical continuation, is shown as a solid blue line. A spline approximation to the boundary computed through direct simulations of the full network (46)-(49) of 1000 neurons is shown as a dotted black line. The red line is rheobase for the uncoupled neuron.

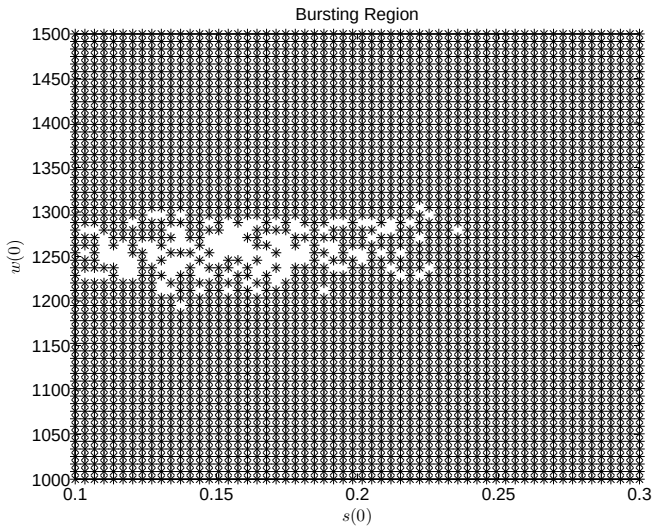

(a) $I_{app} = 1970$ pA

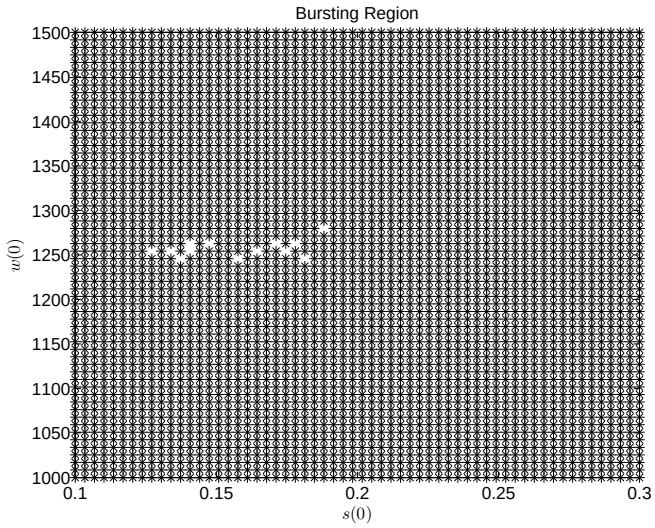

(b) $I_{app} = 1960$ pA

Fig. 6: Evidence for a bistability in the full network (46)-(49). Numerical simulations of the network were run using a 50×50 mesh in the initial values of $s(t)$ and $\langle w \rangle$. Black asterisks indicate bursting, with the white space indicating tonic firing at the mesh point. The conductance parameter is fixed at $g_{syn} = 200$ nS, while the applied current is decreased in increments. The applied current is chosen so that the network is past the bifurcation point to bursting, however remains close to it. A region of bistability is found in the actual network, and this region decreases as we decrease the I_{app} values, eventually disappearing at $I_{app} \approx 1950$ pA. The fuzziness in the region of bistability is partly due to the fact that each neuron in the network is initialized at some resting membrane potential, which has some affect on the region of bistability.

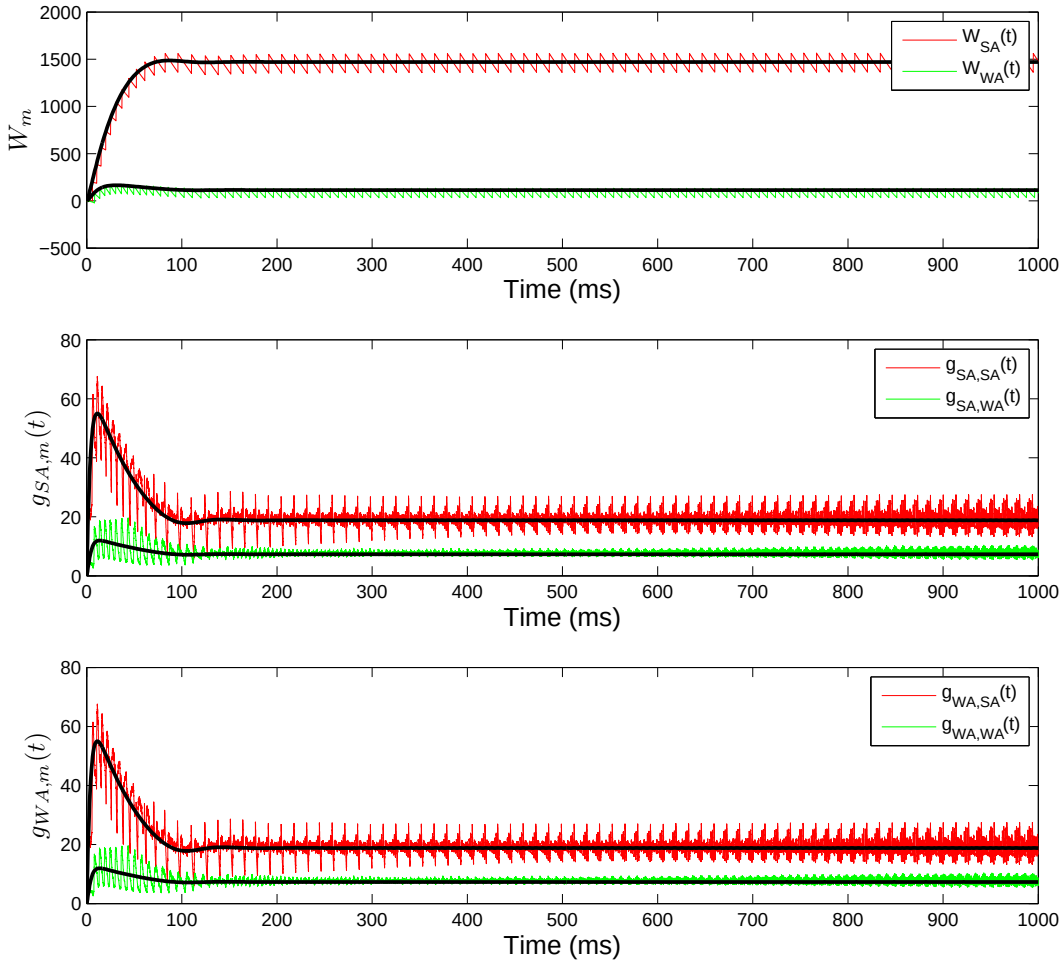

Fig. 7: Comparison of behaviour from numerical simulation of a network of Izhikevich neurons (59)-(62) and of the corresponding mean field model (63)-(66). The network consists of two distinct populations: 800 strongly adapting neurons and 200 weakly adapting neurons. Show in green and red are the population average synaptic conductances, $g_{km}(t)$, and the adaptation current, $W_m(t)$, of a random neuron from each population. Shown in black are the corresponding variables in the mean field model, $g_{syn,km}s_m(t)$ and $\langle w_m \rangle$. The the parameter values can be found in Tables 1-2, except $I_{SA} = 2000$ pA. The network is tonically firing under these parameter settings

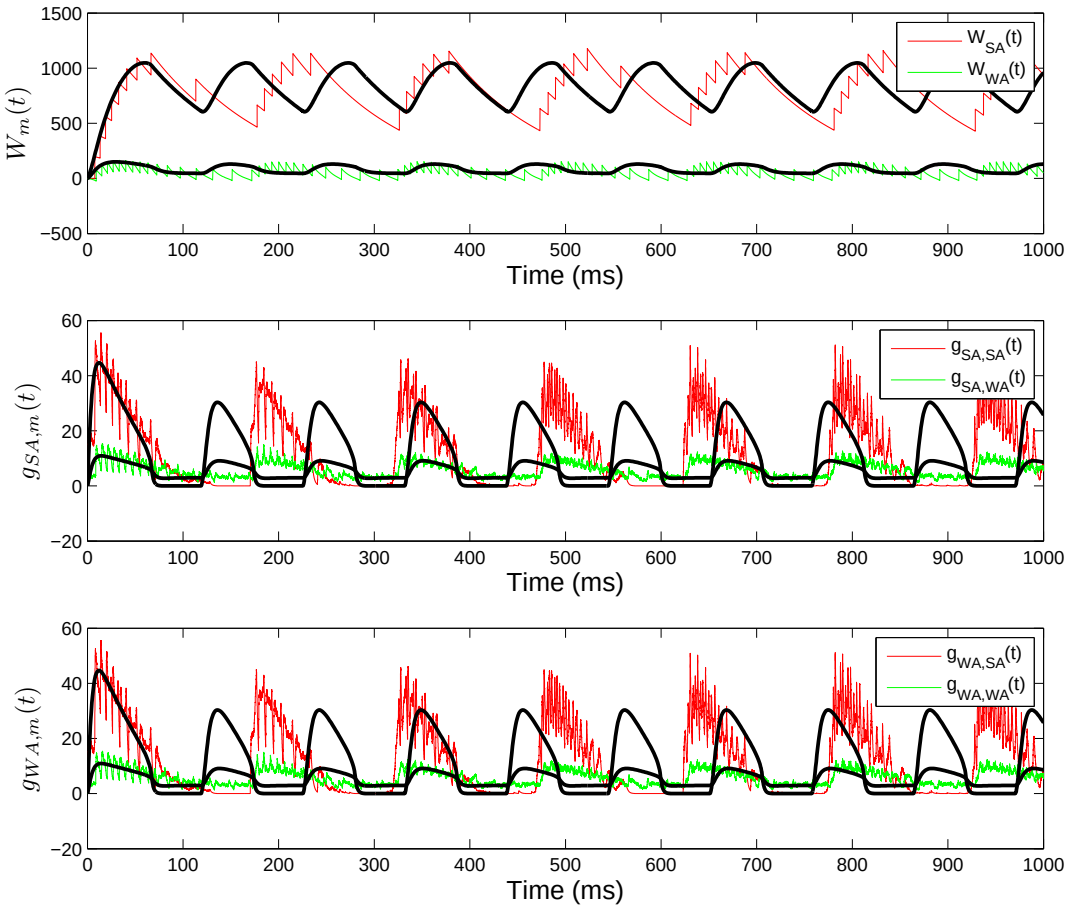

Fig. 8: Comparison of behaviour from numerical simulation of the network of Izhikevich neurons (59)-(62) and of the corresponding mean field model (63)-(66). The network consists of two distinct populations: 800 strongly adapting neurons and 200 weakly adapting neurons. Show in green and red are the population average synaptic conductances, $g_{mk}(t)$, and the adaptation current, $W_k(t)$, of a random neuron from each population. Shown in black are the corresponding variables in the mean field model, $g_{syn,mk}s_k(t)$ and $\langle w_k \rangle$. The parameter values can be found in Tables 1-2, except $I_{SA} = 1500$ pA. The network displays a mixed bursting/oscillatory firing rate. The strongly adapting population is bursting, while the weakly adapting population has an oscillatory non bursting firing rate.

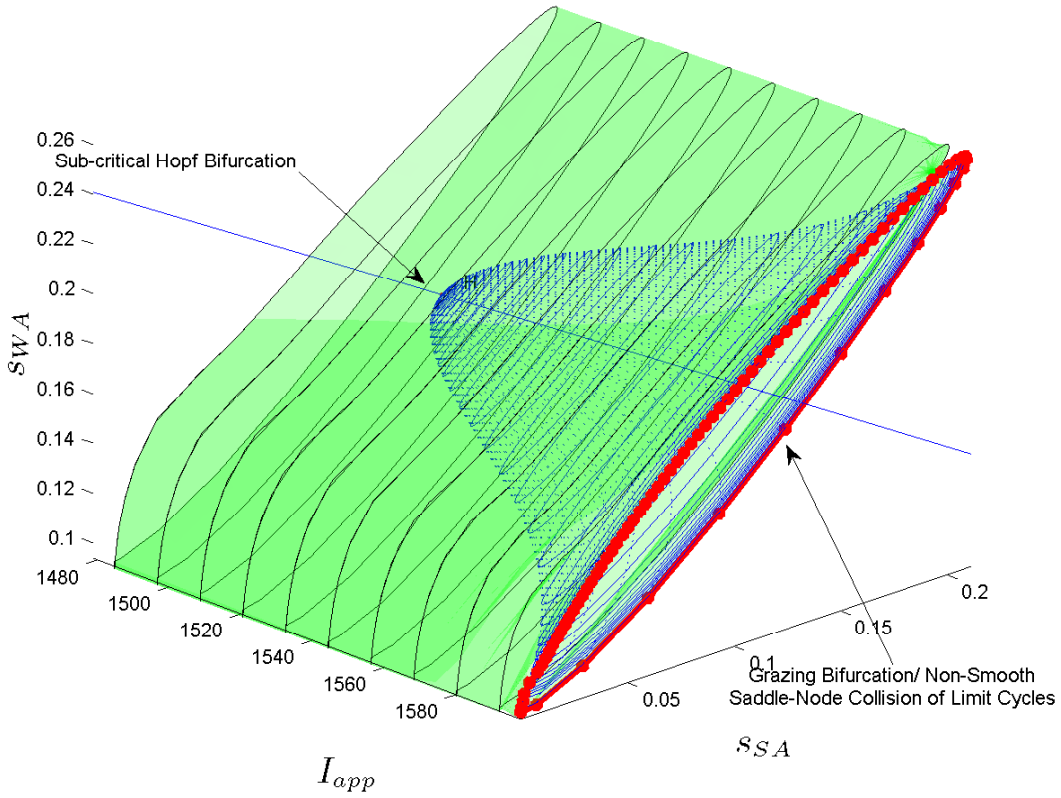

Fig. 9: The bifurcation diagram of the mean field model (63)-(66) for a network consisting of two populations of Izhikevich neurons, one strongly adapting and one weakly adapting. In this diagram, the proportion of strongly adapting neurons was fixed at $p = 0.6$. The subcritical-Hopf limit cycle (blue surface) was computed in MATCONT using standard continuation algorithms. The stable non-smooth limit cycle (green surface) was computed using direct simulations initialized within the basin of attraction for the limit cycle. The tonic firing equilibrium solution is stable for $I > I_{AH}$ and unstable otherwise. A saddle-node collision of limit cycles occurs for $I_{SNC} > I_{AH}$ (near red curve, not shown).

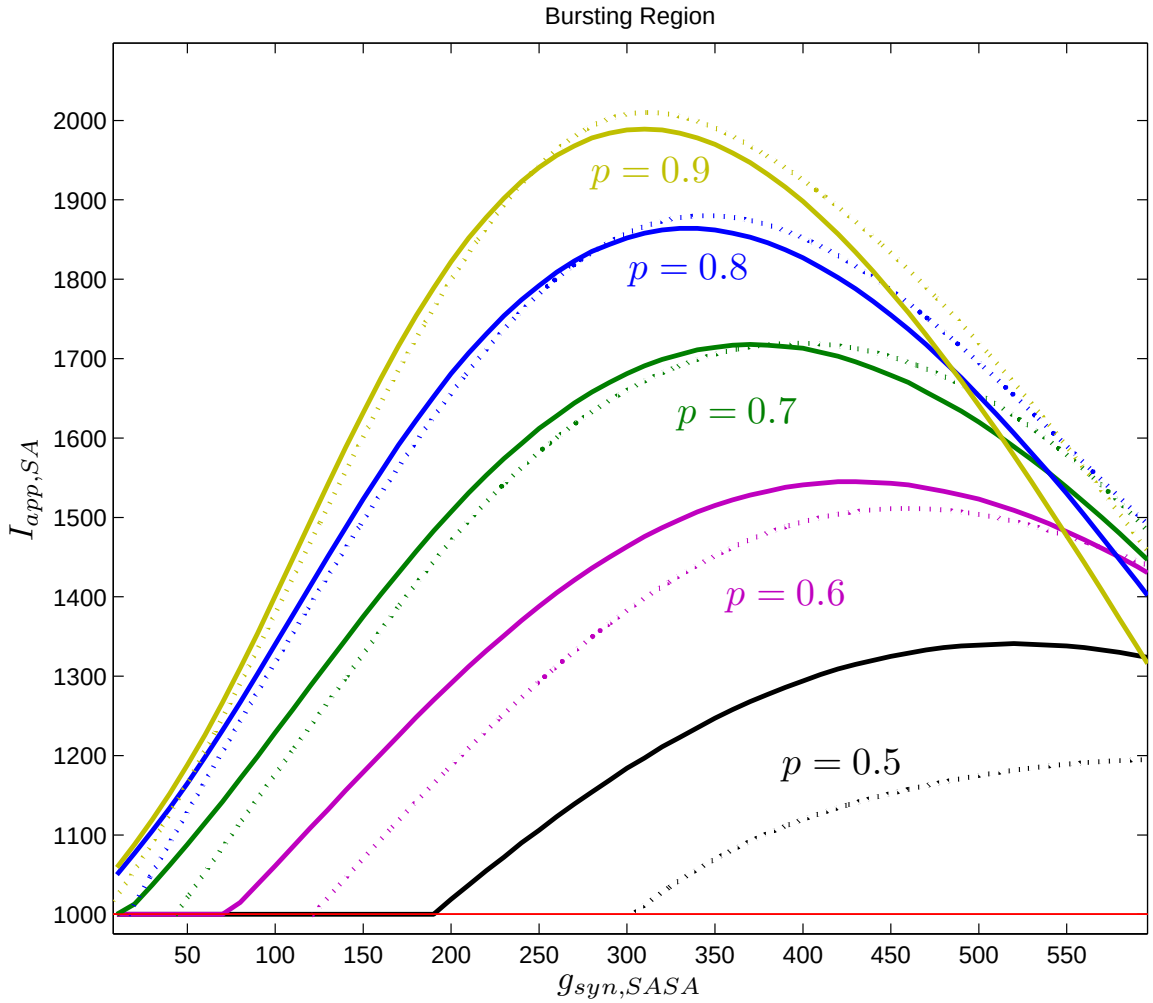

Fig. 10: The Hopf manifolds for the mean field model (63)-(66) (solid lines) in comparison with the boundaries of the bursting region found from direct simulations of the network (59)-(62) over a 2500 point mesh in the parameter space (dotted lines). The proportion of strongly adapting neurons in the network is varied from $p = 0.5$ to $p = 0.9$. Unsurprisingly, larger proportions result in larger bursting regions in the low conductance range.

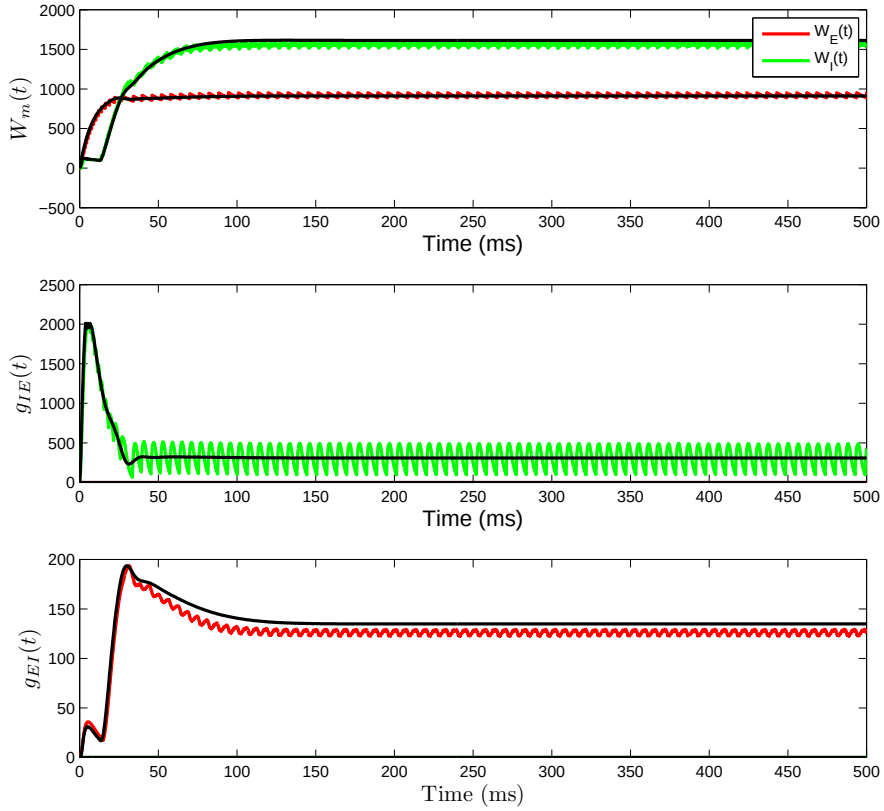

Fig. 11: Comparison of behaviour from numerical simulation of the E/I network of AdEx neurons (70)-(73) (green/red) and of the corresponding mean field model (74)-(79) (black). The network consists of 800 excitatory neurons and 200 inhibitory neurons. The maximal conductances are $g_{EE} = g_{II} = 0$, $g_{EI} = 1000$ nS and $g_{IE} = 2500$ nS. All other parameter values are given in Table 3.

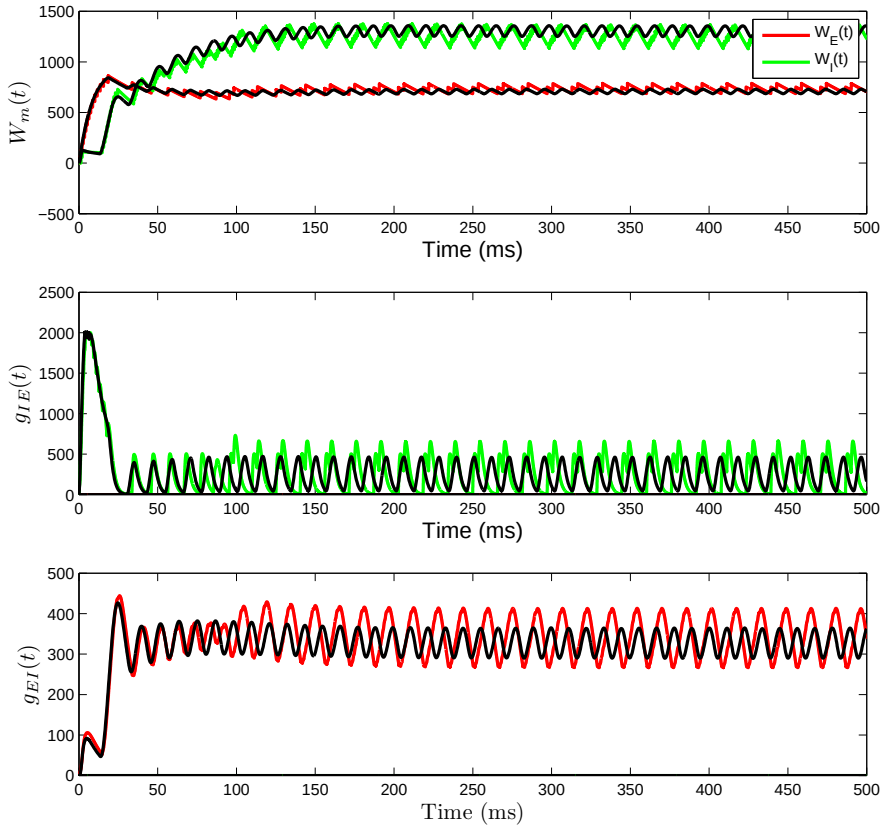

Fig. 12: Comparison of behaviour from numerical simulation of the E/I network of AdEx neurons (70)-(73) (green/red) and of the corresponding mean field model (74)-(79) (black). The network consists of 800 excitatory neurons and 200 inhibitory neurons. The maximal conductances are $g_{EE} = g_{II} = 0$, $g_{EI} = 3000$ nS and $g_{IE} = 2500$ nS. All other parameter values are given in Table 3.

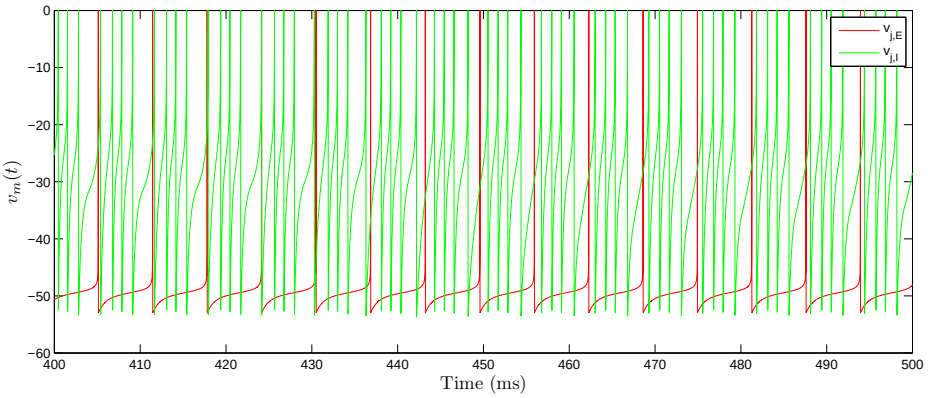

(a) $g_{EE} = g_{II} = 0$, $g_{EI} = 1000$ nS, $g_{IE} = 2500$ nS

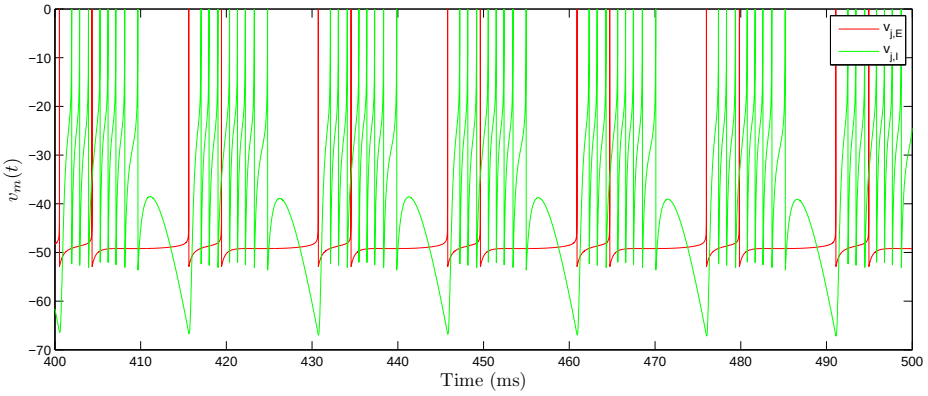

(b) $g_{EE} = g_{II} = 0$, $g_{EI} = 3000$ nS, $g_{IE} = 2500$ nS

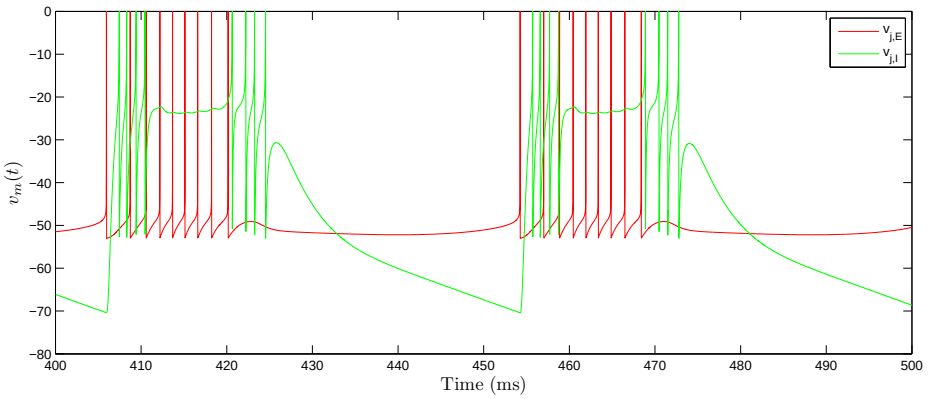

(c) $g_{EE} = 40$ nS, $g_{II} = 1000$ nS, $g_{EI} = 2000$ nS, $g_{IE} = 2000$ nS

Fig. 13: Various firing regimes for the E/I network of AdEx neurons (70)-(73), illustrated by a random neuron from each population. (a) Excitatory population (red) is tonically firing, while inhibitory population (green) is bursting. (b) Excitory population fires doublets, while inhibitory population is bursting. (c) Excitatory population is bursting due to its own recurrent coupling. Inhibitory population exhibits two-phase bursting. Parameter values, other than those indicated, are given in Table 3.

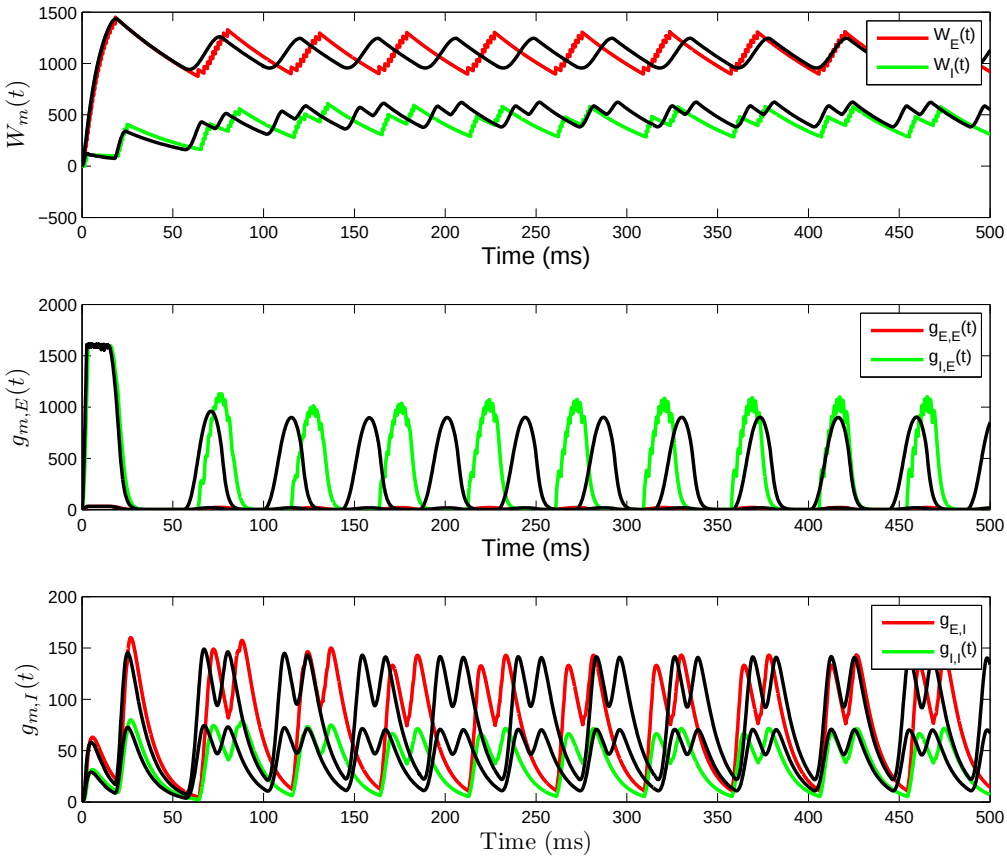

Fig. 14: Comparison of behaviour from numerical simulation of the E/I network of AdEx neurons (70)-(73) (green/red) and of the corresponding mean field model (74)-(79) (black). The network consists of 800 excitatory neurons and 200 inhibitory neurons. The maximal conductances are $g_{EE} = 40$ nS, $g_{II} = 1000$ nS, $g_{EI} = 2000$ nS and $g_{IE} = 2000$ nS. All other parameter values are given in Table 3.